

**PL-TR-97-2023**

# **WIDE-AREA MODELING OF THE IONOSPHERE AND ITS IRREGULARITIES**

**B. W. Reinisch  
G. S. Sales  
J. L. Scali  
X. Huang**

**D. F. Kitrosser  
R. R. Gamache  
R. M. Pickett  
R. I. Brent**

**University of Massachusetts/Lowell  
Center for Atmospheric Research  
Lowell, MA 01854**

**30 December 1996**

**Final Report  
19 April 1990-31 December 1996**

**Approved for public release; distribution unlimited**

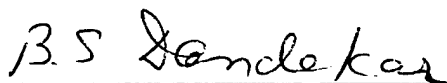


**PHILLIPS LABORATORY  
Directorate of Geophysics  
AIR FORCE MATERIEL COMMAND  
HANSCOM AFB MA 01731-3010**

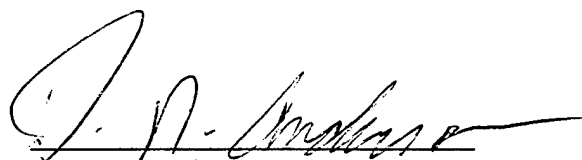
**DTIC QUALITY INSPECTED 3**

**19970430 046**

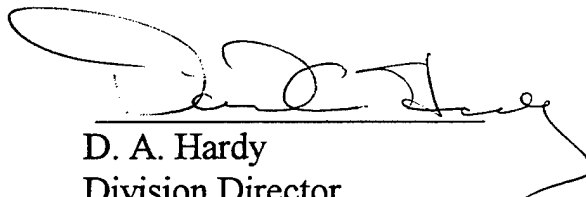
"This technical Report has been approved for publication."



B. S. Dandekar  
Contract Manager  
Ionospheric Applications Branch



D. N. Anderson  
Branch Chief  
Ionospheric Applications Branch



D. A. Hardy  
Division Director  
Ionospheric Effects Division

This report has been reviewed by the ESC Public Affairs Office(PA) and is releasable to the National Technical Information Service (NTIS).

Qualified requestors may obtain additional copies from the Defense Technical Information Center (DTIC). All others should apply to the National Technical Information Service(NTIS).

If your address has changed, if you wish to be removed from the mailing list, or if the addressee is no longer employed by your organization, please notify PL/IM, 29 Randolph Road, Hanscom AFB, MA 01731-3010. This will assist us in maintaining a current mailing list.

Do not return copies of this report unless contractual obligations or notices on a specific document require that it be returned.

REPORT DOCUMENTATION PAGE			Form Approved OMB No. 0704-0188	
Public reporting burden for this collection of information is estimated to average 1 hour per response, including the time for reviewing instructions, searching existing data sources, gathering and maintaining the data needed, and completing and reviewing the collection of information. Send comments regarding this burden estimate or any other aspect of this collection of information, including suggestions for reducing this burden, to Washington Headquarters Services, Directorate for Information Operations and Reports, 1215 Jefferson Davis Highway, Suite 1204, Arlington, VA 22202-4302, and to the Office of Management and Budget, Paperwork Reduction Project (0704-0188), Washington, DC 20503.				
1. AGENCY USE ONLY (Leave Blank)	2. REPORT DATE 30 December 1996	3. REPORT TYPE AND DATES COVERED Final (19 April 1990-31 December 1996)		
4. TITLE AND SUBTITLE Wide-Area Modeling of the Ionosphere and Its Irregularities		5. FUNDING NUMBERS PE 12417F PR ESDO TA 01 WU AB  Contract F19628-90-K-0029		
6. AUTHORS B.W. Reinisch                      X. Huang                      R.M. Pickett G.S. Sales                          D.F. Kitrosser                R.I. Brent J.L. Scali                          R.R. Gamache				
7. PERFORMING ORGANIZATION NAME(S) AND ADDRESS(ES) University of Massachusetts/Lowell Center for Atmospheric Research 600 Suffolk Street Lowell, MA 01854		8. PERFORMING ORGANIZATION REPORT NUMBER		
9. SPONSORING / MONITORING AGENCY NAME(S) AND ADDRESS(ES) Phillips Laboratory 29 Randolph Road Hanscom AFB MA 01731-3010 Contract Manager: Balkrishna S. Dandekar/GPIA		10. SPONSORING / MONITORING AGENCY REPORT NUMBER PL-TR-97-2023		
11. SUPPLEMENTARY NOTES				
12a. DISTRIBUTION / AVAILABILITY STATEMENT Approved for public release; distribution unlimited		12b. DISTRIBUTION CODE		
13. ABSTRACT (Maximum 200 words) This final report covers a wide area of ionospheric research conducted by the Center for Atmospheric Research of the University of Massachusetts in support of the USAF's operational and research interests, the Air Force's global ionospheric sounding network and the Phillips Laboratory Airborne Ionospheric Observatory. The research efforts covered ionospheric modeling and mapping, the study of the physics of the ionosphere in both the polar and equatorial regions and the study of ionospheric structures that range over scales from hundreds of thousands of kilometers at the high end down to small-scale irregularities of the order of tens of meters at the other end of the spectrum.				
14. SUBJECT TERMS Ionospheric Irregularities                      Instruments and Techniques Ionospheric Mapping Equatorial Ionosphere		15. NUMBER OF PAGES 96		
		16. PRICE CODE		
17. SECURITY CLASSIFICATION OF REPORT Unclassified	18. SECURITY CLASSIFICATION OF THIS PAGE Unclassified	19. SECURITY CLASSIFICATION OF ABSTRACT Unclassified	20. LIMITATION OF ABSTRACT SAR	

## TABLE OF CONTENTS

1. INTRODUCTION.....	1
2. OTH RADAR AND COMMUNICATIONS SUPPORT .....	2
2.1 ARTIST Upgrade .....	2
2.2 OTH Radar Test Support .....	5
2.3 Ionospheric Mapping .....	9
2.4 Validation of Ionospheric Models .....	12
2.5 Equatorial Clutter Observations and Analysis.....	25
2.5.1 The UMLCAR Ionospheric Scatter Model.....	25
2.6 OTH Radar Handbook .....	27
3. IONOSPHERIC PLASMA MOTIONS AND ANALYSIS.....	28
3.1 Polar Cap Monitoring.....	28
3.1.1 Introduction.....	28
3.1.2 Calibration of the Digisonde Drift Analysis (DDA) Technique, Using Assumption of Uniform Velocity in the Field-of-View.....	29
3.1.3 The Generalized Digisonde Drift Analysis (GDDA): Measuring the Full Velocity Field.....	32
3.1.4 Determination of the IMF Bz and By Orientations from Digisonde Drift Data.....	44
3.1.5 F-region Polar Cap Convection Pattern.....	46
3.2 Mid-latitude Trough Studies During Geomagnetic Active Periods .....	49
3.3 Equatorial Depletion Bands.....	50
3.4 Geophysical Multi-Instrument Visualization.....	52
4. DIGITAL OBLIQUE REMOTE IONOSPHERIC SENSING .....	53
4.1 Network Synchronization.....	55
4.2 Algorithm Development.....	56
5. JOINT ELECTRONICS WARFARE CENTER PROJECT.....	58
6. DIGISONDE NETWORK SUPPORT.....	65
6.1 April - July 1990 .....	65
6.1.1 Bermuda Naval Air Station (NAS) .....	65
6.1.2 Argentia Naval Air Station (NAS) .....	65
6.1.3 Goose Bay, Labrador .....	66
6.1.4 Airborne Ionospheric Observatory (AIO) .....	66

6.2 August - October 1990 .....	66
6.2.1 Argentia NAS .....	66
6.2.2 Goose Bay, Labrador .....	67
6.2.3 Airborne Ionospheric Observatory .....	68
6.3 November - January 1991 .....	68
6.3.1 Bermuda NAS .....	68
6.3.2 Argentia NAS .....	68
6.3.3 College Station, Alaska .....	68
6.3.4 Sacramento Air Logistics Command .....	69
6.3.5 Goose Bay, Labrador .....	69
6.4 February - April 1991 .....	69
6.4.1 Bermuda NAS .....	69
6.4.2 Argentia NAS .....	70
6.4.3 Goose Bay, Labrador .....	70
6.4.4 Airborne Ionospheric Observatory .....	70
6.5 May - July 1991 .....	71
6.5.1 Bermuda NAS .....	71
6.5.2 Argentia NAS .....	71
6.5.3 Airborne Ionospheric Observatory .....	71
6.6 August - October 1991 .....	72
6.6.1 Bermuda NAS .....	72
6.6.2 Argentia NAS .....	72
6.7 November - January 1992 .....	72
6.7.1 Bermuda NAS .....	72
6.7.2 Argentia NAS .....	73
6.7.3 Qaanaaq, Greenland .....	73
6.7.4 Narssarssuaq, Greenland .....	73
6.8 February - April 1992 .....	73
6.8.1 Bermuda NAS .....	73
6.8.2 Argentia NAS .....	74
6.8.3 Qaanaaq, Greenland .....	74
6.8.4 Narssarssuaq, Greenland .....	75
6.9 May - July 1992 .....	75
6.9.1 Bermuda NAS .....	75
6.9.2 Argentia NAS .....	75
6.9.3 Narssarssuaq, Greenland .....	76
6.9.4 Sondre Stromfjord, Greenland .....	76
6.10 August - October 1992 .....	76
6.10.1 Bermuda NAS .....	76
6.10.2 Argentia NAS .....	77
6.11 November - January 1993 .....	77
6.11.1 Bermuda NAS .....	77
6.11.2 Argentia NAS .....	77
6.12 February - April 1993 .....	78
6.12.1 Bermuda NAS .....	78
6.12.2 Argentia NAS .....	78
6.12.3 Qaanaaq, Greenland .....	78
6.12.4 Sondre Stromfjord, Greenland .....	79

6.12.5 Wallops Island, VA.....	79
6.13 May - July 1993.....	79
6.13.1 Bermuda NAS .....	79
6.13.2 Argentia NAS .....	80
6.14 August - October 1993 .....	80
6.14.1 Bermuda NAS .....	80
6.14.2 Qaanaaq, Greenland.....	80
6.14.3 Narssarssuaq, Greenland.....	81
6.14.4 Sondre Stromfjord, Greenland.....	81
6.15 November - January 1994.....	81
6.15.1 Bermuda NAS .....	81
6.16 February - May 1994.....	82
6.16.1 Bermuda NAS .....	82
6.16.2 Argentia NAS .....	82
6.17 June - August 1994.....	82
6.18 September - November 1994.....	83
6.18.1 Argentia, NAS .....	83
6.18.2 Goose Bay, Labrador.....	83
6.19 December - February 1995.....	83
6.20 March - May 1995 .....	83
6.21 June - August 1995.....	83
6.21.1 Goose Bay, Labrador.....	83
6.21.2 Argentia NAS .....	84
6.22 September - November 1995.....	84
6.22.1 Korea, Osan Air Base.....	84
6.23 December - February 1996.....	85
6.23.1 Bermuda NAS .....	85
6.24 March - May 1996.....	86
6.25 June - August 1996.....	86
7. PUBLICATIONS AND REPORTS FROM THIS CONTRACT .....	86
8. REFERENCES.....	89

*In Memoriam*

Jurgen Buchau  
1933 - 1993

The work described in this Final Report started under the stewardship of Jurgen Buchau, Senior Research Scientist in the Ionospheric Effects Division of the Philips Laboratory at Hanscom AFB, MA. Jurgen Buchau passed away on 9 August 1993. The staff of the Center for Atmospheric Research at the University of Massachusetts Lowell says a last sad farewell to Jurgen with whom they have worked for so many years.

## 1. Introduction

This final report covers a wide area of ionospheric research conducted by the Center for Atmospheric Research of the University of Massachusetts Lowell in support of the USAF's operational and research interests, the Air Force's global ionospheric sounding network and the Phillips Laboratory Airborne Ionospheric Observatory. The research efforts covered ionospheric modeling and mapping, the study of the physics of the ionosphere in both the polar and equatorial regions and the study of ionospheric structures that range over scales from hundreds and thousands of kilometers at the high end down to small-scale irregularities of the order of tens of meters at the other end of the spectrum.

Understanding the dynamics of these regions was an important part of this program and this effort resulted in the development of new powerful tools for analyzing plasma motions in situations where spatial uniformity cannot be assumed. Extensive analyses were carried out, comparing the results of these new techniques with other available sensors to provide these new techniques with the necessary credibility. New software was developed, including an upgraded improved version of our ARTIST program for the automatic scaling of vertical ionograms augmenting the performance of the USAF Digital Ionospheric Sounding System (DISS).

We investigated ionospheric structures that included the mid-latitude trough, polar patches and equatorial depletions bands. New results were obtained that characterize these structures and their effects on radio wave propagation influencing the performance of long range HF communications, VHF/UHF satellite communications and operational Over-The-Horizon radar systems that were an important part of the USAF early warning network. Extensive analysis of radar clutter produced by small scale ionospheric irregularities, particularly in the equatorial regions, was carried out. A new OTH radar clutter model was developed that made it possible to predict the character of the equatorial clutter sources that was almost impossible on the basis of the usual orthogonal backscatter mechanisms.

In addition to this report, the reader is referred to the list (Section 7) of the reports and published papers that were generated under this contract.



## 2. OTH Radar and Communications Support

### 2.1 ARTIST Upgrade

In the early phase of the OTH support program the UMLCAR automatic scaling routine called ARTIST was upgraded. ARTIST is a major software package that automates the scaling of the Digisonde ionograms and the calculation of the true height, i. e. the electron density profiles, in real time and encodes the scaled parameters for transmission to the Air Weather Service for updating their ionospheric models in near real-time to support the OTH operation as well as other users.

The new ARTIST 3 is comprised of 352 subroutines divided into 48 modules. The CIN cross reference numbers and the subroutine names are given in Table 1. Printed copies of the FORTRAN and assembly code for each routine has been produced. Full cross-referencing for calls and calling programs was done for all the routines and noted on the routine cover sheets. Both local and common variable documentation was prepared and checked for each subroutine. Flow charts corresponding to the new subroutines have been created and 206 of these have been put into documentation form.

Table 1. CIN NUMERICAL CROSS REFERENCE

100 ✓ DGSIN=	363 INTDRF=	496 ✓ UNPKP1
110 ✓ MONINP=	365 DRFINT=	497 ✓ CODEPF
120 ✓ IN_MAIN=	370 ✓ MFAC	498 TPKBUF=
	371 ✓ R	
140 ✓ DGSOUT=	372 ✓ GL	500 ✓ PROREC=
150 ✓ MONOUT=	373 ✓ S	505 ✓ UNPREF=
160 ✓ OUT_MAIN=	380 ✓ STPRTN=	515 ✓ CAL_PREQ=
184 ✓ REMOTE=	390 ✓ DISKRD	520 ✓ MOVARY=
200 ✓ EDMENU		
201 ✓ CON_OUT=		
202 ✓ BACK_SPACE=		
204 ✓ CRLF=		
205 CON_IN=		
206 ✓ CLRSCN		
209 CONSRD=	391 ✓ DKCRAM=	521 ✓ MOVEIB=
210 ✓ ARPRINT=	394 DRIFT	522 ✓ MOVDPREF=
220 ✓ SCREEN=	400 ✓ EOFMK	530 ✓ TEST_H_T=
222 CONDCOMD=	401 ✓ READBU=	535 ✓ STMASTR=
224 CONDTTERM=	410 ✓ WFILEM=	540 ✓ CODE_PREF=

Table 1. CIN NUMERICAL CROSS REFERENCE (Continued)

225	CTERM=	411	✓	SPACER=	542	✓	SET_FREQ_	
226	JMD=	420	✓	REWIND=			TAB_PREF=	
228	LOADER=	421	✓	REWIND1=	545	✓	MMM=	
230	SECOND=	430	✓	READTP	546	✓	INITAS=	
232	HARDTIME=	433	✓	WRITBT	547	✓	INTAS6=	
234	PARKDISK=	435	✓	WAITSD	548	✓	CHSARR=	
240	✓	DGSTERM=	437	✓	WRDISK	550	✓	COMPRESS=
250	✓	ROUTE=	438	✓	DISKRM	551	✓	COMP1=
260	✓	AREXEC=	439	✓	MESSAG	555	✓	ELIMN
270	✓	AR256	440	✓	PIFORM	556	✓	SETTAB
271	✓	EDCMD	441	✓	SETTAB	557	✓	INITOL=
305	✓	INITIA	442	✓	PRELUDE	560	✓	CHANST
310	✓	ARIAIB=	443	✓	AMPTSTA	561	✓	STCNVT
315	✓	INITCV	444	✓	STWRTE	579	✓	STOR_IB=
320	✓	INPUT	450	✓	WRITPE	580	✓	COPY_PREF=
321	✓	NUMBER	451	✓	PACKAM	581	✓	COPY_IGSEC=
322	✓	INTFLG	452	✓	PACKDP	600	✓	PROCES
325	✓	ASMINT=	453	✓	GETDCP	601		UTFOF1
330	✓	BUFADR=	455	✓	PKPOWR	602	✓	PFOE
333	✓	STADDR=	456	✓	PKMHZA	603	✓	SUN
335	✓	INT25=	457	✓	PKCOEF	604		FLM
336	✓	DGSINPUT_HANDLER	460	✓	WRITBU=	606	✓	CHKEC2
337	✓	DGS_INPUT	461	✓	WRITE=	608	✓	TCENTR
338	✓	DGS_INT=	470	✓	READMM	609	✓	TCENT2
340		ERRH=	480	✓	CONTRO	610	✓	EREGON
342		NEW_ERR_HANDLER=	482	✓	DOCMD=	611	✓	ETRACE
343		DSPACE=	483	✓	INTAND=	612	✓	ECUSP
344	✓	POLLING_HANDLER=	484	✓	P1BCD	613	✓	PARBOL
345	✓	PORTFLG_ENTRY=	485	✓	P2BCD	614	✓	XTENDE
346	✓	ADD_RTD_TO_AWS=	487	✓	READST=	615	✓	EDOWN
347	✓	BIOS_TIME=	488	✓	READ=	616	✓	FEMIN
348	✓	ASCII_TIME=	489	✓	TIMEOUT=	620	✓	SRANGE
349	✓	STOR_TRAN_TIME=	490	✓	RETURN_STATUS=	622	✓	SFREQ
350	✓	ADD_STRING=	491	✓	DISABLE_DMA=	623	✓	DROPAM
355	✓	SETCHR	492	✓	SETDMA=	624	✓	SUMENG
356	✓	SDATE	493	✓	STATUS=	625		MULTES
360	✓	INIT=	494	✓	WAIT=	626		MAXFES
627		TMPLAT	684	✓	TRACAP	782	✓	DENSTY
628		FILMOR	685	✓	SUMAMP	783	✓	V
630	✓	ES	686		CHK2F	786	✓	HETOF
631	✓	ESWNDW	687		SMTH1F	787	✓	HFITOF
632	✓	ESLIDE	688		FIL1FH	788	✓	GOSUB
633	✓	ESPULF	689		FIL1F	793	✓	CDO
635	✓	FREGON	690	✓	FOFIF	794	✓	SIK

Table 1. CIN NUMERICAL CROSS REFERENCE (Continued)

636 ✓	BASE	691 ✓	SLOPE	795 ✓	DTST
637	RAWBAS	692 ✓	STORXY	796 ✓	ESTAB
638 ✓	BASFLM	693 ✓	LINREG	797 ✓	EQUTN
639	MVHIGH	694 ✓	OVERLP	798 ✓	CHECKH
640	MVLOW	695 ✓	MAXPUL	800 ✓	ULCAR
641	SAVE1F	696 ✓	COPYLN	801 ✓	STAHED
642	BASE1F	697 ✓	SUMIW	802 ✓	PRNFPRF
643	F2GATE	699 ✓	MUFD	808 ✓	SAVREF
644 ✓	BASE2	700 ✓	DOPAM	809	MESSAG
645 ✓	DEFLM	701 ✓	MEDAMP	810	HOURLY
646 ✓	UPLIMT	702 ✓	DOPAMP	811 ✓	UPDATE
647 ✓	UPLMT2	703 ✓	CALMHZ	812 ✓	ASHIFT
648 ✓	SUMBS	704 ✓	STRAMP	813 ✓	K24HED
649 ✓	SMOTH2	705 ✓	MEDIAN	814 ✓	TIM2PN
650 ✓	DFOF2	710 ✓	PROFILE	820 ✓	AWS
651 ✓	STCUSP	711 ✓	SETCV	821 ✓	QLETTER
652 ✓	SMOOTH	712 ✓	SETRCE	822 ✓	STHEAD
653 ✓	MINF	713 ✓	FILLGAP	823 ✓	INTCHAR
654 ✓	MINHT	714 ✓	LINRP	825 ✓	STIONL
655 ✓	EFGAP	715 ✓	SHIFTP	826 ✓	FILBLN
656 ✓	SCFOF1	716 ✓	RSORT	835 ✓	PLOTRC
657 ✓	FTLOW	717	PMGAP	836 ✓	PLOTR2
658 ✓	FITCFQ	718	FINDSH	841 ✓	BUMARK
659 ✓	TUNEF2	719	MCSTART	842 ✓	CNTLSQ
660 ✓	OBLIQ	720 ✓	DECIDE	843 ✓	COMPRS
661 ✓	ETCHK	721 ✓	EPROF	890 ✓	PNTCRL=
662 ✓	SET999	722 ✓	TRIONS	891 ✓	INTCR2
663 ✓	FNDJJO	723 ✓	FNDDHE	895	WRCOEF
664 ✓	HYPSTF	724 ✓	FNDDHW	896	AWSCOE
665 ✓	HYPERB	725 ✓	FNDFL	903 ✓	COPYBU
666 ✓	MED	726 ✓	F1PROF	904 ✓	ENDBUF
667 ✓	FILLZ	727 ✓	ZLOWER	909 ✓	INITAR
668	CHEKBS	728 ✓	FPROP	910 ✓	MILSEC=
669 ✓	BSSTAT	730 ✓	CHKMON	916 ✓	SETUPD=
670 ✓	SRCH20	731 ✓	MPM	917 ✓	PORTFLG_FOR=
671 ✓	SUMHYP	732 ✓	POLVAL	918 ✓	SIGFIG
672 ✓	MINHT2	733	ESRSS	919 ✓	STCRLF=
673 ✓	REPEAT	735 ✓	VIRTUAL	921 ✓	SWAP
674 ✓	CHKE2	736 ✓	PROF	922 ✓	SORT
675 ✓	FDOWNP	737 ✓	TSTAR	930	CMPTIM
		738 ✓	PAHP	931	CHGTIM
				932	SETTIM

Table 1. CIN NUMERICAL CROSS REFERENCE (Continued)

676 ✓ FPLUSE	739 ✓ PWHP	933 ALLSE
677 ✓ FINALE	740 ROOTER	940 DGSADR=
678 ✓ SHRNKE	741 PBFIT	945 GETDAT=
680 ✓ PREDTE	742 DTSTAR	946 SEND_
681 ✓ PEDGE	750 ✓ CONVKM	COMMAND=
682 ✓ PULFIT	770 ✓ TABLE2	947 CHECK_TIME_
683 ✓ SUMIA	781 ✓ SETUP	MODE=
950 DGSCMD=	1000 CHEKB2	948 WAITSC=
955 ATTIME=	1001 CHEKB3	1010 ✓ BSPULSE
956 DECIMAL_TO_BCD=	1002 CHEKB4	1011 ✓ BSPUL2
957 JULIAN_DAY=	1003 CHEKB5	1012 ✓ BSPUL3
958 UNPACK_AT_DATE=	1004 CHEKB6	1015 ✓ CKBSHT
		1018 ✓ CKMINF

The completed Version 1.1 of the ARTIST software was installed on the depot mock-up DISS Digisonde at Sacramento ALC and a one day training session was provided to the depot personnel on the installation procedures. The personnel also received an associated technical briefing on the AN/FMQ-12. After operating the new software, a few minor discrepancies were noted which postponed final deployment of the software. In January 1990, these corrections were implemented into Version 1.2 and in-house testing of the software began. Before finalizing the ARTIST software a field test of the software on an operational AN/FMQ-12, such as Wallops Island, VA, was considered and a request for authorization to operate the Wallops Island system using the Version 1.2 software was forwarded to the program office at Sacramento ALC.

In March 1991, Version 1.2 of the ARTIST software was installed on the operational DISS systems at Wallops Island, VA and Vandenberg AFB, CA. The software was installed for the purpose of testing the software before acceptance on the part of the Air Force. The ARTIST software was operated successfully at both the Wallops Island and Vandenberg DISS stations and no discrepancies were reported.

## 2.2 OTH Radar Test Support

With the beginning of the West Coast OTH radar system (WCRS) operation, the UMLCAR support effort was extended to this system in addition to the east coast (ECRS) radar system. A first visit to the WCRS at Mountain Home AFB, Idaho took place in August 1990 to observe the radar system in operation in preparation for the test flights scheduled for October 1990.

UMLCAR's part in the Air Force "test and evaluation" of the WCRS involved spending one week at the operations site located at Mountain Home, ID. During this period approximately eight Phillips Laboratory (PL) aircraft flights were scheduled, flying different patterns in support of the Air Force test program. The visit offered the opportunity to observe the environmental assessment (EA) operators and to better understand the problems that they face at this site which might be different from those at the ECRS which lies much closer to the auroral region. Although the effects of auroral activity are considerably less at the WCRS than at the ECRS, the effects of the equatorial clutter on the performance of the radar are as dramatic and possibly even greater, as the performance of the WCRS in the daytime is so much better than at the ECRS and the contrast makes the equatorial problem more apparent.

During these flights a routine data collection system was set up to gather hard copy of as much of the EA displays as was possible. Primarily, this included the routine backscatter (BS) ionograms, the clutter-to-noise ratios and the ionospheric parameter maps for foF2, foE, etc. These maps of the ionospheric characteristics serve to improve the modeling of the ionosphere for the EA coordinate registration task. UMLCAR personnel also were aboard the Phillips Laboratory aircraft during these missions and supported the flight planning, data gathering and equipment maintenance.

The radar also provided the Amplitude-Range-Doppler (ARD) data recorded on magnetic tape and hard copy. The tapes contain the received Doppler frequency spectra as a function of range for each scan of the radar making it possible to recover the ionospheric clutter spectra associated with the nighttime equatorial activity. These data were used to build the clutter model describing the effects of equatorial clutter on the radar's performance.

In addition to the campaigns at the WCRS, a routine data collection effort was carried out at the ECRS to provide the data set necessary for understanding the characteristics of equatorial clutter. To process the large amount of data generated for the ECRS synoptic study of equatorial clutter, typically storing one hour of radar operation on one radar magnetic tape, the individual ARD spectra were compressed reducing the 64 or 128 Doppler amplitude points to a set of 8 quantities that describe the key parameters of each spectrum. These compressed spectra were stored separately from the main database on an Exobyte recorder and used for the synoptic analysis of the equatorial clutter. This data compression by a factor of the order of ten and the use of the Exobyte made it possible to store three months of spectra (one season) on a single tape.

A special analysis was carried out to determine the optimum set of parameters required to characterize individual ARD spectra so that it would be possible to reconstruct the spectrum with reasonable fidelity. The details of the algorithm were published in a technical report (Sales, 1992). Eight parameters were identified as follows:

1. ground clutter peak amplitude
2. ground clutter peak Doppler frequency
3. ionospheric clutter peak amplitude
4. ionospheric clutter peak Doppler shift
5. ionospheric clutter slope (left of peak)
6. ionospheric clutter slope (right of peak)
7. noise level (transmitter on)
8. noise level (transmitter off)

This approach was based on the assumption that the ionospheric clutter spectra have two different characteristic shapes, very often appearing as triangular or flat spectra across the Doppler frequency range.

After discussions with MITRE and Rome Laboratory, the other participants in the test program, it was decided that all participating groups standardize their analysis and displays for Silicon Graphics work stations. This fitted in well with our approach for autoproccessing of the ARD database and being able to retrieve and display the various data forms. The initial output of the autoproccessing were 2-D range/azimuth contour plots of the several scaled parameters. The algorithm development worked well and only relatively minor changes had to be made to improve its performance. The improvement process continued until the parameterization program worked very well with only few occasional failures. This approach was acceptable considering the cost, in time and effort, for developing a totally error free algorithm. Since one year's ARD data were processed, failures are smoothed over and disappear within the large database.

Using the programming resources of RADEX (Mr. Douglas Reynolds), it has been possible to display the calculated scattering cross section of 3-D ionospheric irregularities in all directions, including forward scatter. Application to the equatorial clutter problem has yielded good results using reasonable values for the intensity of the irregularities ( $\Delta N/N=0.1$  to  $0.3$ ) and a correlation ellipsoid axial ratio of the order of  $10^4$ . During the US-Australia OTH meeting in March 1993, Dr.

Michael Kelley of Cornell University suggested, on the basis of a recent thesis by D. Hysell, that axial ratios of the order of  $10^5$  and  $10^6$  were more appropriate in the equatorial region. Implementing these numbers produced a problem for the very weak backscatter (BS) in the equatorial regions and required looking into the forward scatter as an alternative.

Several visits to the two radar operations sites and retroactive analysis confirmed that the EA operators did not fully understand the structure of the backscatter ionograms, often confusing the several components that make up the structure of the BS ionograms. To provide a teaching aid to the operators UMLCAR developed a backscatter ionogram synthesis program using 3-D ray tracing along with the best available ionospheric model. The current choice are the models produced by Dr. David Anderson, Phillips Laboratory, and his group. A side benefit of our use of these models is their evaluation and the detection of their weaknesses/errors. These observations were fed back to Dr. Anderson and his contractors.

The backscatter ionogram synthesis allowed us to investigate the mechanism for the "hard traces" often observed on the actual ionograms produced at the radar when looking towards the equatorial region. These flat (constant range) traces occur as a result of strong focusing of the sounder energy after crossing an elevated ionospheric region such as that across the magnetic equator in the early nighttime period. A complete sequence of these ionograms was generated and compared with the actual soundings. The results were presented at the joint US-Australia radar meetings.

An important part of this effort was to correlate the backscatter ionogram observations of these hard traces with radar clutter. Until this time a relationship has only been suspected on the basis of a few examples but the connection had not been established. One reason is that the radar ARD data is always range ambiguous and any meaningful analysis must unfold the radar clutter observations. For this purpose we developed a range ambiguity chart that allows radar operators and analysts to quickly determine the possible ranges associated with the clutter.

Problems kept appearing in the auto-processor program as large quantities of data were processed. Some cases do not have the expected noise minimum at the extreme Doppler frequency corresponding to  $\pm 1/2$  of the waveform repetition frequency. In other cases the mean noise level gradually increased from the shortest range to the longest. Both of these problems and others were solved, one at a time, with the goal in mind to keep the algorithm as simple as possible and the processing time as short as possible. The resulting processor was reasonably robust, compressing the ARD data by almost a factor of 500 without losing any important part of the database.

Geographic displays on the Silicon Graphics System were developed to display the sources of ionospheric clutter in the range interval where they likely originate. The range folding associated with the pulsed waveform of the radar makes the clutter measurements ambiguous and some intuition must be used to resolve this problem. The displays facilitated the analysis and helped in the unscrambling process. As part of the scatter model effort, the 3-D anisotropic scattering model was applied to the bistatic ROTH - JORN measurements, looking for areas where enhanced scatter might occur. The conditions for specularity were calculated, again with the help of D. Reynolds of RADEX. Results of this work were presented to the joint US/Australia OTH working group in May 1993, including the first results for the January 1992 nine day campaign. A final report describing this autoscaling algorithm was prepared jointly by RADEX and the University of Massachusetts Lowell Center for Atmospheric Research.

Different displays were developed for the nine day ECRS January 1992 campaign to present the data. The focus of the analysis was directed towards the amplitude and Doppler spectrum width of the ionospheric clutter that directly affects the performance of the radar. The best technique was to compress all ranges and present the data as azimuth versus time. Most of the nine consecutive days were from Segment III from 20UT to 04UT, i.e. from around sunset through local midnight. The strongest clutter appeared around sunset and to the east of the present Segment III coverage. It was concluded that the strong clutter from the east corresponds to the transition from ground scatter from the South American land area (near Argentina/Uruguay border around the southern anomaly region) to the sea where the backscatter is significantly larger. The analysis of bistatic sea scatter, i.e. scatter where the incoming wave has a different direction from the scattered wave, predicts 23dB loss compared to direct backscatter from the sea at low angles, in good agreement with the observations.

### **2.3 Ionospheric Mapping**

This investigation was aimed at developing techniques for improved modeling of the ionosphere in the radar's coverage region based on vertical sounder data from the Digisonde network that supports the EA function of the radar. Jurgen Buchau of the Phillips Laboratory had identified problems with the ionospheric model updating, some of which were so severe that the usefulness of such models was very limited. Reliable techniques of mapping the ionosphere over a limited geographical region using a network of vertical incidence (VI) sounders needed to be developed. For the ECRS the network consists of five Digisonde sites located within the coverage region of the ECRS: Goose Bay, Labrador; Argentia, NF; Millstone Hill, MA; Wallops Island, VA and on



Bermuda Island. These VI sounders form a relatively closely spaced network which can be used to predict, in real-time, the layer parameters anywhere within the region defined by these sites.

Different approaches were considered for the generation of better ionospheric models. The type of connecting surface had to be selected for optimally interpolating the particular ionospheric parameter from the sounder points to grid points where no measurement were made. The surface will depend on the weights given to each sounder point. It is clear that the spatial correlation function should control the weights to be applied to each sounder measurement. If the field point is sufficiently far from a particular sounder then the measured value at that sounder has little influence on the value for the field point. This can be affected by making the weights depend directly on the assumed correlation between the two separated points. Initially the correlation function developed by Rush [1972] for an earlier global ionospheric study was used.

As a corollary to the question of the best correlation function to be used in the process of calculating the weights, an additional requirement was established designed to ensure that the measured parameters at each of the sounding sites (Goose Bay, Argentina, Bangor, Wallops Island, Bermuda, and the UMLCAR sounder at Millstone Hill) are faithfully reproduced in the resulting maps of the ionosphere. This requirement is based on the assumption that the actual measurements at each site have zero error associated with them. The set of weights is given by:

$$W_{ij} = \frac{r_{ij}^2}{1 - r_{ij}^2} \quad (1)$$

where  $r_{ij}$  is the correlation coefficient, and the weighted value of the particular parameter  $h_j$  at the field point is given in terms of the  $N$  measured values  $h_i$  and their associated weights as:

$$h_j = \frac{\sum_{i=1}^N W_{ij} h_i}{\sum_{i=1}^N W_{ij}} \quad (2)$$

As the field point approaches one of the sounders, the associated weight becomes very large, approaching infinity as the correlation approaches unity. This large weight dominates all the others and these others can be neglected. Then the large weight, the same in the numerator and in the

denominator, cancel and the interpolated value approaches the measured value as the field point approaches the sounder point.

Using this general approach, techniques were developed for mapping the ionosphere in the specified region as defined by the OTH radar requirement to sound over the 180° coverage of the ECRS. Reviewing these concepts with the Air Force scientists, it was recognized that the sphere of influence of certain sounders should be limited because the geophysical character of one observation point may be completely unrelated to far away grid points. For example, the auroral nighttime values of foF2 at Goose Bay should not significantly influence the value at field grid points south of the trough.

Our initial approach to this problem was the choice of the character of the correlation ellipse associated with each station, and considering contour shapes other than an ellipse. In the auroral zone, ellipses were used with high axial ratios and with the major axis extending approximately magnetically east-west along the auroral oval. It was found that this did not sufficiently limit the range of influence of the auroral (Goose Bay) soundings and the next attempt was to introduce a family of "evolute" curves to further enhance only the east-west extension of the correlation influence. After trying a series of these somewhat ad hoc approaches to the generation of the ionospheric parameters map, it became apparent that this technique basically forced the interpolated map to fit the preconceived idea. This approach was therefore abandoned.

A different technique was developed by Capt. J. Wojtal [1991] as part of his Masters thesis. This technique calculates the spatial correlation coefficients between the pairs of sounders yielding the correlation coefficient for the various distances and in the different directions. For each of the five sounding stations there are four correlation coefficients. It was assumed that the spatial variation of the correlation coefficient could be described as a Gaussian function with one initially unspecified parameter, the scale length in the particular direction from the "base" station to each of the other four sounders. In order to improve the estimate of the correlation coefficient, Wojtal used the data from the four hours prior to the "current" time for the last eight days, i. e. 32 samples, to calculate the correlation coefficient. This had the effect of smoothing some of the variations and also of sometimes combining the data from before and after the sunrise and sunset transition periods. Wojtal's technique finds the lengths and directions of the major and minor axes of the ellipse for each station. These correlation ellipses from the five sounder data set were then used to determine a set of weights applied to each of the measured ionospheric parameters from the five stations to estimate the value at an arbitrary location in the local field. The results were not better than the initial Rush approach, and the technique was not pursued.

The search for a method that was not model based resulted in a unique and powerful concept for real-time mapping that has the potential for predicting the electron density distribution, at least for several hours into the future. For an extended area, the local time at different sites is different and this must be considered when the surfaces are constructed. The new method uses the time history of profiles at each of the sounder locations within the region to be mapped.

Prof. X. Huang developed algorithms that use the time series of soundings at each station to determine the amplitude and phase of the spectrum components with periods of up to 16 hours. Then, the same spectrum component is fit across the array of sounders to find the amplitude and direction of the spatial wave component that best fits these data. After determining the characteristics of these spatial waves for each of the profile parameters, they can be combined at any arbitrary location to determine the profile at this grid point. Preliminary results of this study were presented at the IRI Modeling Workshop at Athens, Greece in October 1991 [Reinisch et al., 1993], and at the Solar Terrestrial Predictions Workshop at Ottawa, Canada in May 1992.

The concept used is based on the understanding that many of the changes in the ionosphere over a local region are correlated over reasonable distances and can be described in terms of large scale ionospheric wave-like movements passing through the area. The amplitude, phase, direction and velocity of the spectrum of the waves passing over the coverage is determined using the 24 to 36 hour time history of the vertical profiles, taken at 30 minute (or shorter) intervals at each sounding station. The spectrum of best fit "spatial waves" are then combined to represent the electron density profile at any selected point within the mapped region. For short term prediction, these same waves can be "propagated into the future" and again be combined to represent the ionosphere as it would likely to appear at that time. Several tests were carried out to evaluate the mapping technique and they indicate that the method works quite well and is recommended for OTH precision targeting.

## **2.4 Validation of Ionospheric Models**

The validation of ionospheric models began with the need to assess how well these models reproduced the characteristics observed in the ionosphere. In recent years many models, theoretical and empirical, had been developed, however no extensive comparison between the modeled values and the experimental measurements were made. This in part was due to the time involved in extracting ionospheric profiles from existing conventional ionograms. In some cases scaled characteristics such as foF2, foE were compared however due to the complexity of inverting the ionograms to true height profiles, the electron density profiles were not readily available.

With the advent of digital ionosondes and in particular the sophistication of the Digisonde, it was finally possible to construct a database which contained a complete description of the bottomside ionosphere for use in comparison with the models. At a business meeting of the Ionospheric Informatics Working Group (IIWG of URSI) held on 3 October 1991 in Athens, it was agreed to organize a program for the validation of ionospheric models (VIM). For the purpose of constructing this VIM database, at the beginning of 1992, UMLCAR began reprocessing data from the Digisondes at Millstone Hill, Bermuda and Wallops Island. Although at the time the Digisonde automatically scaled and inverted the ionogram to true height, the supplied ionospheric parameters had an accuracy rated at 90-93%, it was decided to reprocess the datasets to provide the modelers with the most unambiguous dataset, where the accuracy was closer to 100%.

Initially, the VIM database consisted of reprocessed Digisonde data obtained during the months of March 1990, June 1990, October 1989 and December 1990. These periods were considered since data existed for all the stations listed above, and the effect of seasonal variability in the models could be checked. At the PRIME/URSI workshop in Roquetes, Spain (spring 1992), the first comparison of the electron density profiles derived from ionograms with the three ionospheric models, IRI, PLIM, and FLIP were presented [Reinisch et al., 1994]. The results presented to the ionospheric community illustrated the performance of the ionospheric models, the need for more comparison work, and the importance of the VIM database.

The development of the VIM database at UMLCAR continued and expanded to include Digisonde systems operating at Argentia (Newfoundland), Cachoeira Paulista (Brazil), Dourbes (Belgium), Goose Bay (Labrador), Kirtland AFB (NM), Qaanaaq (Greenland) and San Diego (CA). In January 1993, at the URSI/PRIMO workshop in Boulder, CO, results of the PRIMO/VIM Digisonde data for solar maximum was presented. During this meeting, the status of the VIM database was discussed. It was decided that the parameters NmF1, hmF1 and half-height  $h(1/2 \cdot \text{NmF2})$  should be included in the VIM datasets. The inclusion of the half-height would require modification to the in-house programs ARTIST [Reinisch and Huang, 1993], ADEP [Adep Manual 1994], NHPC and VIM developed at UMLCAR. The model validation results are described in a paper by Anderson et al., [1996].

To assure the accuracy of the Digisonde profile data, UMLCAR continued comparing the electron density profiles with other techniques and improving the inversion techniques. Hence, on modifying the programs for inclusion of the half-height for VIM, the profile inversion algorithm in ARTIST, ADEP and NHPC were also modified, using an improved valley model. This valley model is described by a width and a depth which is recorded and archived in the ADEP database

files. The data collected in the VIM database were reprocessed with these latest programs, and were distributed to Dr. David Andersen at Phillips Laboratory, Utah State University and the World Data Center A (WDC-A) Boulder Colorado for inclusion into the CD archive of geophysical data. The current list of data is shown in Table 2 and contains data from 10 stations spanning some six years of measurements.

Table 2. VIM Data in the WDC-A Database

A1089.VIM	D0290.VIM	K1089.VIM	Q0189.VIM
A0390.VIM	D0390.VIM	K0390.VIM	
A0590.VIM	D0690.VIM	K0690.VIM	SD0392.VIM
A0690.VIM	D1190.VIM	K1290.VIM	
A0890.VIM	D1290.VIM		W0788.VIM
A1190.VIM		M0388.VIM	W0590.VIM
A1290.VIM	G1089.VIM	M1288.VIM	W0690.VIM
	G0390.VIM	M0789.VIM	W1089.VIM
B1089.VIM	G0590.VIM	M1089.VIM	W1190.VIM
B0590.VIM	G0690.VIM	M0190.VIM	W1290.VIM
B0690.VIM	G0890.VIM	M0290.VIM	
B1190.VIM	G1190.VIM	M0390.VIM	
B1290.VIM	G1290.VIM	M0590.VIM	
		M0690.VIM	
		M0790.VIM	
BRZ1292.VIM		M0890.VIM	
BRZ0693.VIM		M1190.VIM	
		M1290.VIM	
		M1292.VIM	

The filenames have the following description; the initial letter (or letters) stands for the station name. The first 2 numbers are the month and the next 2 numbers are the year. The extension is .VIM The station information is written in the files. The letter codes are: (A) Argentina, Newfoundland, (B) Bermuda, (BRZ) Brazil, (D) Dourbes, Belgium, (G) Goose Bay. Labrador, (K) Kirtland AFB, (M) Millstone Hill, MA, (Q) Qaanaaq, Greenland, (SD) San Diego, CA, (W) Wallops Island.

Additional VIM data were processed for a five month period from December 1991 to April 1992 for the stations Goose Bay, Millstone Hill and Ramey (Puerto Rico). The data tapes for these

months and stations were obtained from the World Data Center-A. ADEP SURVEYs were run on these data tapes to indicate the days for which data exist. After studying the SURVEY output, data were selected where all three stations have good data for at least 5 consecutive days. Unfortunately, in December 1991 and April 1992 there was no period where all three stations had data. Table 3 displays the completed dataset in which data were available.

Table 3. List of days for edited ionospheric data from Goose Bay, Ramey and Millstone Hill Digisonde stations

GOOSEBAY DATA				
Dec. 1991	Jan 1992	Feb. 1992	Mar 1992	Apr 1992
341	24	46	86	109
344	25	47	87	110
345	26	48	88	111
346	27	49	89	112
	28	50	90	113
			91	
RAMEY DATA				
Dec. 1991	Jan 1992	Feb 1992	Mar 1992	Apr 1992
340	24	46	86	No data
341	25	47	87	--
344	26	48	88	--
345	27	49	89	--
346	28	50	90	--
			91	--
MILLSTONE HILL DATA				
Dec 1991	Jan 1992	Feb 1992	Mar 1992	Apr 1992
No data	24	46	86	109
--	25	47	87	110
--	26	48	88	111
--	27	49	89	112
--	28	50	90	113
--			91	

Another period for developing a VIM database involved processing a whole month of data for each season from October 1992 to December 1993. The months chosen were October, December 1992, March, June October and December 1993 for Goose Bay, Ramey, Millstone Hill, Wallops Island, Puerto Madryn (Argentina) and Jicamarca. These VIM datasets are listed in Table 4. The shaded days represent those days where data were manually edited. Approximately 44% of the data gathered at UMLCAR for processing and inclusion in the VIM database have been edited.

Table 4. VIM Database Edited Data Status

GOOSEBAY DATA					
Oct. 1992	Dec. 1992	Mar. 1993	June 1993	Oct. 1993	Dec. 1993
275	336	60	152	274	335
276	337	61	153	275	336
277	338	62	154	276	337
278	339	63	155	277	338
279	340	64	156	278	339
280	341	65	157	279	340
281	342	66	158	280	341
282	343	67	159	281	342
283	344	68	160	282	343
284	345	69	161	283	344
285	346	70	162	284	345
286	347	71	163	285	346
287	348	72	164	286	347
288	349	73	165	287	348
289	350	74	166	288	349
290	351	75	167	289	350
291	352	76	168	290	351
292	353	77	169	291	352
293	354	78	170	292	353
294	355	79	171	293	354
295	356	80	172	294	355
296	357	81	173	295	356
297	358	82	174	296	357
298	359	83	175	297	358
299	360	84	176	298	359
300	361	85	177	299	360

Table 4. VIM Database Edited Data Status (Continued)

301	362	86	178	300	361
302	363	87	179	301	362
303	364	88	180	302	363
304	365	89	181	303	364
305	366	90		304	365
RAMEY DATA					
Oct. 1992	Dec. 1992	Mar. 1993	June 1993	Oct. 1993	Dec. 1993
275	336	60	152	274	335
276	337	61	153	275	336
277	338	62	154	276	337
278	339	63	155	277	338
279	340	64	156	278	339
280	341	65	157	279	340
281	342	66	158	280	341
282	343	67	159	281	342
283	344	68	160	282	343
284	345	69	161	283	344
285	346	70	162	284	345
286	347	71	163	285	346
287	348	72	164	286	347
288	349	73	165	287	348
289	350	74	166	288	349
290	351	75	167	289	350
291	352	76	168	290	351
292	353	77	169	291	352
293	354	78	170	292	353
294	355	79	171	293	354
295	356	80	172	294	355
296	357	81	173	295	356
297	358	82	174	296	357
298	359	83	175	297	358
299	360	84	176	298	359
300	361	85	177	299	360
301	362	86	178	300	361
302	363	87	179	301	362
303	364	88	180	302	363
304	365	89	181	303	364
305	366	90		304	365



Table 4. VIM Database Edited Data Status (Continued)

MILLSTONE HILL DATA					
Oct. 1992	Dec. 1992	Mar. 1993	June 1993	Oct. 1993	Dec. 1993
275	336	60	152	274	335
276	337	61	153	275	336
277	338	62	154	276	337
278	339	63	155	277	338
279	340	64	156	278	339
280	341	65	157	279	340
281	342	66	158	280	341
282	343	67	159	281	342
283	344	68	160	282	343
284	345	69	161	283	344
285	346 ND	70	162	284	345
286	347 ND	71	163	285	346
287	348 ND	72	164	286	347
288	349 ND	73	165	287	348
289	350 ND	74	166	288	349
290	351 ND	75	167	289	350
291 ND	352 ND	76	168	290	351
292 ND	353 ND	77	169	291	352
293	354 ND	78	170	292	353
294	355 ND	79	171	293	354
295	356 ND	80	172	294	355
296	357	81	173	295	356
297	358	82	174	296	357
298	359	83	175	297	358
299	360	84	176	298	359
300	361	85	177	299	360
301	362	86	178	300	361
302	363	87	179	301	362
303	364	88	180	302	363
304	365	89	181	303	364
305	366	90		304	365
WALLOPS ISLAND DATA					
Oct. 1992	Dec. 1992	Mar. 1993	June 1993	Oct. 1993	Dec. 1993
275	336	60	152	274	335
276	337	61	153	275	336
277	338	62	154	276	337
278	339	63	155	277	338
279	340	64	156	278	339
280	341	65	157	279	340

Table 4. VIM Database Edited Data Status (Continued)

WALLOPS ISLAND DATA					
Oct. 1992	Dec. 1992	Mar. 1993	June 1993	Oct. 1993	Dec. 1993
281	342	66	158	280	341
282	343	67	159	281	342
283	344	68	160	282	343
284	345	69	161	283	344
285	346	70	162	284	345
286	347	71	163	285	346
287	348	72	164	286	347
288	349	73	165	287	348
289	350	74	166	288	349
290	351	75	167	289	350
291	352	76	168	290	351
292	353	77	169	291	352
293	354	78	170	292	353
294	355	79	171	293	354
295	356	80	172	294	355
296	357	81	173	295	356
297	358	82	174	296	357
298	359	83	175	297	358
299	360	84	176	298	359
300	361	85	177	299	360
301	362	86	178	300	361
302	363	87	179	301	362
303	364	88	180	302	363
304	365	89	181	303	364
305	366	90		304	365
PUERTO MADRYN DATA					
Oct. 1992	Dec. 1992	Mar. 1993	June 1993	Oct. 1993	Dec. 1993
275 ND	336 ND	60	152 ND	274 ND	335 ND
276 ND	337 ND	61	153 ND	275 ND	336 ND
277 ND	338 ND	62	154 ND	276 ND	337 ND
278 ND	339 ND	63	155 ND	277 ND	338
279 ND	340 ND	64	156	278 ND	339
280 ND	341 ND	65	157	279 ND	340
281 ND	342 ND	66	158 ND	280 ND	341
282 ND	343 ND	67	159 ND	281 ND	342
283 ND	344 ND	68 ND	160 ND	282 ND	343
284 ND	345 ND	69	161 ND	283 ND	344
285 ND	346 ND	70	162 ND	284 ND	345
286 ND	347 ND	71	163	285 ND	346

Table 4. VIM Database Edited Data Status (Continued)

PUERTO MADRYN DATA (Cont.)					
Oct. 1992	Dec. 1992	Mar. 1993	June 1993	Oct. 1993	Dec. 1993
287 ND	348 ND	72	164	286 ND	347
288 ND	349 ND	73	165	287 ND	348 ND
289 ND	350 ND	74	166 ND	288 ND	349 ND
290 ND	351 ND	75	167	289 ND	350 ND
291 ND	352 ND	76 ND	168	290 ND	351
292 ND	353 ND	77	169	291 ND	352 ND
293 ND	354 ND	78 ND	170	292 ND	353 ND
294 ND	355 ND	79 ND	171 ND	293 ND	354
295 ND	356 ND	80	172 ND	294 ND	355
296 ND	357 ND	81	173 ND	295 ND	356 ND
297 ND	358 ND	82 ND	174 ND	296 ND	357
298 ND	359 ND	83 ND	175	297 ND	358
299 ND	360 ND	84 ND	176	298 ND	359
300 ND	361 ND	85 ND	177 ND	299 ND	360
301 ND	362 ND	86 ND	178 ND	300 ND	361
302 ND	363 ND	87 ND	179 ND	301 ND	362
303 ND	364 ND	88 ND	180 ND	302 ND	363
304 ND	365 ND	89 ND	181 ND	303 ND	364
305 ND	366 ND	90 ND		304 ND	365 ND
JICAMARCA DATA					
Oct. 1992	Dec. 1992	Mar. 1993	June 1993	Oct. 1993	Dec. 1993
275	336	60	152	274	335
276	337	61	153	275	336
277	338	62	154	276	337
278	339	63	155	277	338
279	340	64	156	278	339
280	341	65	157	279	340
281	342	66	158	280	341
282	343	67	159	281	342
283	344	68	160	282	343
284	345	69	161	283	344
285	346	70	162	284	345
286	347	71	163	285	346
287	348	72	164	286	347
288	349	73	165	287	348
289	350	74	166	288	349
290	351	75	167	289	350
291	352	76	168	290	351
292	353	77	169	291	352

Table 4. VIM Database Edited Data Status (Continued)

JICAMARCA DATA					
Oct. 1992	Dec. 1992	Mar. 1993	June 1993	Oct. 1993	Dec. 1993
293	354	78	170	292	353
294	355	79	171	293	354
295	356	80	172	294	355
296	357	81	173	295	356
297	358	82	174	296	357
298	359	83	175	297	358
299	360	84	176	298	359
300	361	85	177	299	360
301	362	86	178	300	361
302	363	87	179	301	362
303	364	88	180	302	363
304	365	89	181	303	364
305	366	90		304	365

The VIM data format originally adopted was very similar in structure to the standard station monthly characteristics report format files, but only the VIM parameters were present. This format was presented in the report by Gamache and Reinisch [1991].

With the UMLCAR database center coming on-line in August 1994 all datasets processed were stored in the Standard ADEP Output (SAO) format. This format was first presented at the IIWG Lowell workshop on "Digital Ionogram Data Format for the World Data Center" [Gamache and Reinisch, 1989]. This format was developed so that :

- (a) The data format could handle measurements for which the number of data varies from record to record.
- (b) To minimize the size of the data file.
- (c) To be flexible enough for future enhancements.

It was decided that all processed datasets housed in the UMLCAR data center, including the VIM database would be stored in the SAO format. These files contain the complete information for the ionospheric parameters and form the basis for standardizing in the exchange of data. All the processed datasets listed in Tables 3 and 4 have been saved in the UMLCAR database in the SAO format. All these files were stored on the first UMLCAR data center CD-ROM generated. The UMLCAR data center CD contains over 270 Mbytes of edited Digisonde data collected at 15

Digisonde stations. UMLCAR has already started collection of a new set of Digisonde processed data for producing the next CD-ROM.

Since its first development and presentation in 1989, the SAO data format has met with great success and was adopted by URSI as a recommended international standard for archiving edited ionogram data. Throughout the years the format of the SAO database has evolved as the needs arose. The format was enhanced to consider higher resolution data and was incorporated into the UMass Lowell ARTIST, ADEP, NHPC, and VIEWER [Digisonde Portable Sounder Commercial Manual, 1996] programs. The SAO file format allows the user to specify the URSI station number [Piggott and Rawer, 1978] or the UMass Lowell station ID codes.

The UMASS Lowell ID codes were updated to avoid conflicts in datasets collected at Digisondes sharing the same latitude, however located at different longitudes. This new labeling scheme was adopted to uniquely code the data to a particular station using a 3-digit code. The last two digits are the integer latitude of the station. The value is obtained by rounding the latitude to an integer by the scientific procedure of rounding numbers and not the method used in some FORTRAN program compilers, thus 34.7 becomes 35. The first digit in the code identifies the hemisphere the station is in. A "0" is used to label the northern hemisphere and a "9" is used to label the southern hemisphere. Stations at the same latitude are assigned numbers from zero upward in the northern hemisphere and from nine downward in the southern hemisphere. For example, the stations at Karachi (Pakistan) and Chung-Li (Taiwan) are at 25.0 N, 67.1 E and 25.0 N, 121.2E, respectively. To distinguish these stations the first is labeled 025 and the second 125. A third station at 25N would take the label 225 and so forth. In Table 5 are the stations in the Worldwide Digisonde Network with their coordinates, old IDs and the new station ID values. This information may assist the AF Space Forecast Division to decide which sites should participate in their global network.

Table 5. Stations and their ID codes in the Worldwide Digisonde Network

Station Name	Old I.D.	Geographic Latitude	Geographic Longitude	New I.D.	System
Zhong-Shan (Antarctica)	069	69.2 S	76.2 E	969	DPS-4
Casey Base (Antarctica)	066	66.3 S	110.5 E	966	DPS-4
Puerto Madryn (Argentina)	042	42.7 S	294.7 E	943	DPS-1
Beverage, La Trobe (Australia)	045	37.8 S	145.0 E	938	DGS-256
Salisbury DSTO (Australia)	034	34.7 S	138.6 E	935	DPS-1
Pietersburg (S. Africa)	261	24.0 S	29.5 E	926	DPS-4
Alexander Bay (S. Africa)	N/A	28.6 S	16.5 E	929	DPS-4
Grahamstown (S. Africa)	N/A	33.3 S	26.5 E	933	DPS-4
Cachoeria (Brazil)	023	23.2 S	314.2 E	923	DGS-256
Learmonth (Australia)	097	21.8 S	114.0 E	922	DISS
Elliott (Australia)	018	17.6 S	133.5 E	918	DPS-1
Darwin NT (Australia)	012	12.5 S	130.9 E	913	DPS-1
Jicamarca (Peru)	012	12.0 S	283.2 E	912	DPS-1
Pontianak (Indonesia)	001	0.3 S	109.0 E	900	DPS-1
Ramey (Puerto Rico)	042	18.5 N	292.9 E	019	DISS
Maui, Hawaii	090	20.8 N	203.5 E	021	DISS
Karachi (Pakistan)	025	25.0 N	67.1 E	025	DGS-256
Chung-Li (Taiwan)	025	25.0 N	121.2 E	125	DPS-1
Okinawa (Japan)	026	26.3 N	127.8 E	026	DPS-1
Eglin AFB, FL	084	30.4 N	273.2 E	030	DISS
Wuhan (China)	030	30.6 N	114.3 E	031	DGS-256
Bermuda NAS	089	32.4 N	295.3 E	032	DISS
Dyess AFB, TX	098	32.5 N	260.3 E	033	DISS
Islamabad (Pakistan)	034	33.8 N	72.9 E	034	DGS-256
Vandenberg AFB	091	34.7 N	239.4 E	235	DISS
Kirtland AFB	033	35.1 N	253.4 E	135	DGS-256
Xinxiang (China)	035	35.3 N	113.9 E	035	DGS-256
Kokubunji (Japan)	036	35.7 N	139.5 E	036	DGS-256
El Arenosillo (Spain)	040	37.1 N	353.3 E	037	DGS-256

Table 5. Stations and their ID codes in the Worldwide Digisonde Network (Continued)

Station Name	Old I.D.	Geographic Latitude	Geographic Longitude	New I.D.	System
Anyang (Korea)	037	37.4 N	127.0 E	137	DGS-256
Wallops Is. (USA)	081	37.9 N	284.5 E	038	DISS
Athens (Greece)	038	38.0 N	23.6 E	138	DGS-128
Sacramento (USA)		38.5 N	238.5 E	039	DISS
Beijing (China)	039	39.9 N	116.5 E	040	DGS-256
Kuson (Korea)	096	40.3 N	128.7 E	140	DISS
Roquetes (Spain)	041	40.8 N	0.3 E	041	DGS-256
Roma (Italy)	048	41.9 N	12.5 E	042	DGS-256
Millstone Hill	042	42.6 N	288.5 E	043	DGS-256
Argentia Nfd. (Canada)	047	47.3 N	306.0 E	047	DISS
Dourbes (Belgium)	049	50.1 N	4.6 E	050	DGS-256
Amchitka, AL	093	51.4 N	179.2	051	DISS
Slough (England)	051	51.5 N	359.4 E	052	DPS-1
Goose Bay (Labrador)	057	53.3 N	299.7 E	053	DISS
Lerwick (Shetland Is. UK)	061	60.1 N	358.8 E	060	DPS-1
Narssarssuaq (Greenland)		61.2 N	314.6 E	061	DISS
College Alaska (USA)	082	64.9 N	212.2 E	065	DISS
Sondrestrom (Greenland)	067	67.0 N	310.0 E	067	DISS
Tromso (Norway)	042	69.9 N	19.2 E	070	DPS-4
Qaanaaq (Greenland)	077	77.5 N	290.6 E	078	DGS-256
Svalbard (Norway)	079	78.9 N	11.9 E	079	DPS-4
Polarstern Expedition	099	ship	ship		DGS-256
DSTO #4		mobile	mobile		DPS-1

## **2.5 Equatorial Clutter Observations and Analysis**

During special meetings at Phillips Laboratory experts from the Air Force, MITRE, UMLCAR and other interested organizations discussed the feasibility of making definitive measurements to improve the understanding of the sources of equatorial clutter and their effects on the radar's performance. Consideration was given to hold field campaigns using either the ECRS or the WCRS or both depending on the time frame and the availability of the two radars for the investigation into the sources of equatorial clutter. These campaigns were carried out in the spring and fall of 1991 and involved the Geophysics Laboratory Airborne Ionospheric Observatory. We also began investigating possible scatter mechanisms for producing radar backscatter clutter from the equatorial region. The UMLCAR scattering model was adapted to the numerical ray trace program with good results in spite of the fact that it is in general not possible to achieve orthogonality with the field aligned irregularities at these low magnetic latitudes. This issue is discussed later.

The equatorial clutter measurements made at the WCRS during the October 1990 campaign served to characterize the different kinds of Doppler spectra that are commonly observed at the radar sites from the equatorial irregularities. The radar observations are concentrated in time from the early evening during the onset of the equatorial clutter, as the sunset terminator moved into Segment I of the radar, until sunrise so as to track the decay of these clutter sources as the sun rises on the easterly regions as seen from the WCRS. These campaigns were conducted on several nights and excellent data were obtained.

### **2.5.1 The UMLCAR Ionospheric Scatter Model**

The ionospheric scatter model developed by G. S. Sales was attached to a ray tracing program, thereby combining the results of the ray tracing in terms of angles the rays make with the earth's magnetic field allowing realistic backscatter calculations. In order to assess the expected clutter levels produced by these models, typical cases were considered in terms of range and azimuth for the likely clutter sources. Such sources include auroral, equatorial and weaker midlatitude irregularities using the geometries appropriate for both the ECRS and the WCRS and then computing the backscattered power. These explicit calculations, carried out over a reasonable range of elevation angles, used the ray tracing program. The results explain the observed clutter level on the basis of scattering from a power law irregularity spectrum of intensities of the order of  $\Delta N/N = 0.1$  in the auroral region, up to  $\Delta N/N = 0.3$  in the region where the equatorial plumes reach down into the lower ionosphere (at  $\pm 20^\circ$  from the magnetic equator in the anomaly regions) at altitudes around 200 to 300 km, i.e. below the F-region peak.



This scattering model does not require special conditions for the angles that the rays make with the field aligned irregularity structure. For the typical case with a spectral index  $n = -2$ , sufficient power is backscattered, with a high power OTH radar, to be observed. The calculated backscattered powers are consistent with the observations from the U.S. radars. Orthogonality is not required to explain the radar clutter observed in the coverage regions. The ionospheric clutter frequently observed on the backscatter ionograms in the 1/2 hop region with the relatively low power backscatter sounder is a manifestation of the stronger orthogonal clutter.

Using the reformulated program for calculating the expected clutter levels by backscatter from a power law distribution of ionospheric irregularities, it has been observed that sufficient power is returned to the radar from the angular scatter spectrum at arbitrary angles and does neither require orthogonality nor specular conditions to be satisfied. Of course, if and when these special conditions are satisfied the backscattered power is large. Although this often occurs at locations (ranges) that are not of great interest in terms of their effect on radar target detection, it is of great importance to the low power HF diagnostic radars that are often used for scientific studies of auroral/equatorial irregularities. This "low" level clutter is often within 10 or 20 dB of the ground clutter amplitude and under certain conditions can be as great as the ground clutter. This ionospheric clutter is relatively isotropic and is therefore distinctly different from the usually highly aspect sensitive clutter that arises from orthogonal/specular type scatter.

Using reasonable estimates for the intensity (RMS) of the fluctuations in electron density, the expected backscattered power of 104 dBW was calculated from both the auroral and equatorial regions. The results are very encouraging for the equatorial clutter problem, in particular, since it has been shown that special conditions such as orthogonality and specularity are very difficult, if not impossible, to achieve at low latitudes where the earth's magnetic field is almost parallel to the surface of the earth, without introducing great contortions of the ray path. The calculations demonstrated that equatorial clutter (low power) is not an unusual event and only requires the presence of small scale irregularities, such as those normally connected with spread F occurrences.

Considerable effort has been expended in the scaling of the ARD data from the earlier WCRS campaign to determine some of the characteristics of the equatorial clutter as observed by the radar. This was accomplished by measuring the clutter levels at three points in the spectrum:

1. any ionospheric clutter peak found near the 0 Hz portion of the spectrum,
2. at a point half-way between 0 Hz and the outer limit of the spectrum, i.e. at WRF/4,

3. at the outer limit of the spectrum, i.e. at  $WRF/2$ .

The data for several runs through the sunset and sunrise periods were plotted to determine when the equatorial clutter appears to begin and end. UMLCAR's earlier work on scattering, both forward and backscatter from random distributions of anisotropically distributed electron density fluctuations, was improved by using a bispectral distribution, with the power law distribution changing from  $n = -2$  for large wavenumbers to  $n = -4$  at a selected transition wavenumber. This change in the model was based on criticism that the observed fluctuation spectra often seemed to show this kind of change in the spectrum index. This modification did not alter the previous conclusion that equatorial clutter originates from spread F irregularities not requiring orthogonality with the magnetic field.

UMLCAR personnel, together with Jurgen Buchau and his team at Phillips Laboratory, acquired a large database during extensive campaigns of the equatorial clutter phenomenon using the WCRS. Hard copies of backscatter ionograms, ionospheric parameters and the amplitude-range Doppler formatted output made it possible to quantify the ionospheric clutter originating in the region around the magnetic equator in terms of backscattered power and Doppler spectra. Detailed analyses of the character of these Doppler spectra showed the geographical distributions of the clutter sources in the equatorial regions and their temporal behavior. It was established that these clutter problems often appear before sunset and persist until after sunrise in a particular radar beam. This had not been predicted by the satellite scintillation measurements made in the past in these equatorial regions. The scintillations begin after sunset and usually diminish around midnight. It appears that the transionospheric satellite measurements indicate only the formation of intense equatorial plumes while the more sensitive radar observations are mainly affected by the more pervasive equatorial bottomside spread F.

## **2.6 OTH Radar Handbook**

UMLCAR participated in the production of a basic "handbook" for the OTH radar operators. During many visits to the sites it was found that the operators were often trained by their associates and in this process misinformation was passed on from "generation to generation". A handbook was required to cover all aspects of the radar operation and particularly the interaction of the radar with the ionosphere. UMLCAR prepared two sections of the handbook on "Radar System" and "Radio Wave Propagation". These sections were designed to provide the operators with the basics of radar technology and HF radio wave propagation in an ionized medium.

A draft of these two sections was prepared by G. S. Sales and submitted to the Air Force OTH program office for their review. Upon the recommendation of the program office and their consultants at the MITRE Corporation additional material was included, in particular examples of real data to illustrate the concepts. To improve the backscatter ionogram simulations the effects of ionospheric clutter were included requiring the use of analytic ray tracing. A model of the earth's magnetic field was incorporated to determine where the rays are perpendicular to the field-aligned irregularities producing strong backscatter clutter.

After an extensive review by the OTH community, including Rome Laboratories, MITRE Corp. and ESD, UMLCAR updated and expanded the two Chapters and published them in two Air Force reports. A review of several of the other chapters was also provided.

### **3. Ionospheric Plasma Motions and Analysis**

#### **3.1 Polar Cap Monitoring**

##### **3.1.1 Introduction**

In trying to understand the electrodynamic system set up in the high latitude region due to the interaction of the Interplanetary Magnetic Field (IMF) with the ionosphere, several empirical and mathematical models have been developed to map out the convection patterns which describe plasma transport processes [Sojka et al., 1986; Heppner and Maynard 1987; Hairston and Heelis, 1990]. In order to specify the convection patterns precisely, these models require, as a minimum, inputs for the orientation of the IMF (sign of  $B_z$  and  $B_y$  components), the position of the daytime cusp and the nighttime Harang discontinuity regions. The essential advantage of these models lies in their ability to specify the real time convection patterns. In order to do this, real time data gathering of the required IMF and high latitude ionospheric responses is needed.

The Polar Cap Monitoring (PCM) initiative was designed to use a network of groundbased observation stations (i.e. digital ionosondes), which are capable of measuring and tracking rapid changes in the orientation of the IMF,  $B_z$  and  $B_y$  components [Reinisch et al., 1987; Cannon et al., 1991] and the ionospheric behavior to these changes. Digisondes are low maintenance, continuously operating systems that measure electron densities and plasma velocities, and provide the data in real time which can be used as input for the specifications and requirements of the convection models. Before implementing the PCM concept, several exploratory studies needed to be done:

- (a) Calibration of Velocity Data. The Digisonde uses Doppler interferometry techniques to locate the reflection source locations and uses these to determine a 3D velocity vector from the

Doppler and source location information. As such, the determined velocities represent a composite of the motion of plasma irregularities and changes in the reflecting medium. An understanding of how well this Digisonde "apparent velocity" represented the true plasma motion in the polar and high latitude regions was required.

(b) Determination of IMF orientation. It was necessary to determine the orientation of the IMF Bz and By components from the Digisonde velocity data. Due to the high correlation in changes in the plasma velocities and IMF reversals, it was proposed to develop a scheme that could determine the orientation of the IMF Bz and By components using velocities measured by Digisondes in the polar region.

(c) Polar Cap Convection Pattern. Combine models and Digisonde velocities to produce polar circulation patterns to determine if the PCM concept was feasible, making use of IMP8 IMF measurements for comparison.

These studies not only verified the Digisonde velocity technique as a very powerful tool for monitoring convection patterns in the polar region, but also led to 1) a better understanding of the complexities in measuring velocities in these regions, 2) a better interpretation of what motions were really measured by other instruments, and 3) the development of an improved drift analysis technique titled the Generalized Digisonde Drift Analysis (GDDA) method. The following sections discuss the areas of studies under the PCM initiative and their results.

### **3.1.2 Calibration of the Digisonde Drift Analysis (DDA) Technique, Using Assumption of Uniform Velocity in the Field-of-View.**

While the Digisonde drift analysis method has been used extensively in the high latitude regions to interpret the ionization convection patterns [Reinisch et al., 1987, Buchau et al., 1988; Cannon et al., 1991; Crowley et al., 1992] no detailed analysis has been published on how well the apparent velocities represented the real plasma velocity at these latitudes. Akram [1992] comparing Digisonde (DGS) drift speeds measured at 300 km and velocities measured from the DMSP satellite showed that the DGS velocities were consistently lower than the satellite value by a factor varying between 0.3 and 0.5. Several mechanisms to account for the discrepancy were discussed, but no explanation was really satisfactory.

Using velocity measurements made by a Digisonde and an incoherent scatter radar (ISR) colocated at Sondre Stromfjord, Greenland, a detailed analysis of the velocity techniques was made and results were compared. The ISR database consisted of 232 hours of ISR data from 6 runs covering the period from August 1991 to March 1992. The Digisonde ran continuously in a 15-

minute schedule and had data available for each day during this period. From this data set a specific period was chosen between 5 to 9 December 1991, when the IMF data were also available, the two instruments were operating well and the integrity of the data processed was good for both instruments. The instrumentation setup and data acquisition specifics for this time period are given in the following descriptions.

Station :                      Sondre Stromfjord (Greenland)  
Coordinates :              67.0 N,              309.1 E              (Geographic)  
Inclination :              80.37 (Alt. 250 km, IGRF)  
Declination :              -38.77 (Alt. 250 km, IGRF)  
Data Period :              5 to 9 December 1991

#### Incoherent Scatter Radar

Measurement: Doppler line-of-sight velocities were measured for approximately 5 minutes (dwell time) at three fixed beam positions which are given by their azimuth (Az) and Zenith (Zen) as:

Beam 1 :              Az = 141°              Zen. = 10°  
Beam 2 :              Az = 261°              Zen. = 20°  
Beam 3 :              Az = 21°              Zen. = 20°

Including antenna positioning, a full set of dwells was obtained in 17 minutes, at which time a 3D velocity vector was calculated. Therefore, for each height sampled an average velocity is calculated approximately once every 17 minutes.

#### Digisonde 256

Measurement: Doppler line-of-sight velocities were measured for a single frequency and four ranges (one drift case) every 5.12 seconds. A group of approximately 20 drift cases were recorded every 5 minutes. Using the Digisonde Drift Analysis (DDA) technique [Reinisch et al., 1995; Scali et al., 1995], generally over 1500 reflection location regions and their associated line-of-sight velocities are obtained within a two-minute period. A velocity distribution is obtained every 5 minutes. With DDA the velocities are calculated assuming spatial uniformity in the plasma motion.

Since the Digisonde sample heights were determined by the ionospheric characteristics at the time of observation, it was important to properly interpret these height variations when comparing with the ISR velocities. At mid-to-low latitudes where the horizontal plasma velocity can vary as a function of height due to ion-drag, it was very important that the ISR and DGS velocities be compared at the same sampling height. At higher latitudes, the effect of electric fields mapping from high altitudes becomes dominant and the plasma motion is mainly controlled by the  $\mathbf{E} \times \mathbf{B}$  drift, and therefore should be height independent. To check that the velocities at Sondre Stromfjord are height independent, an analysis on the ISR velocities was done to check for possible velocity height gradients.

The velocity difference distributions for  $V_{\perp N}$  and  $V_{\perp E}$  components observed over five ISR sampling heights were obtained by subtracting the velocities measured at a reference ISR height of 198 km. These statistics include all the ISR velocities measured during 5 to 9 December 1991 and show that from 198 to 438 km, the mean differences in the velocities (not considering their error estimates) measured at each height varied by 19 m/s for the  $V_{\perp N}$  components and 34 m/s for the  $V_{\perp E}$  components. Considering that at Sondre Stromfjord the velocity magnitudes are usually of the order of several hundreds of meters per second, the mean differences observed are negligible. This is not to say that a velocity dependence with height does not exist, differences with height can at times be observed. However, with standard deviations in the distributions of 91 and 171 m/s for the  $V_{\perp N}$  and  $V_{\perp E}$  components, these differences are comparable with the error estimates of the ISR and DGS systems which at times are as large as 200 m/s. Hence for our comparisons, in general, we assumed that the velocities measured at Sondre Stromfjord were height independent.

The ISR and DGS velocities for each day from 5 to 9 December 1991 (Days 339 to 343) were compared. The ISR velocities were averaged over the height range from 198 to 438 km and only this average value was used. The Digisonde, 5-minute median velocities were smoothed by a 5 point triangular weighted running average. The overall comparison of the ISR and DGS velocities is quite good. The apparent velocities measured by the Digisonde at Sondre Stromfjord reproduced the velocity variations observed by the ISR. Even fast velocity changes were similar for the two instruments.

The close agreement between the velocities measured by the two techniques is even more apparent when the average over the five days are used (Figure 1a and b). The transition across the day side cusp at 13 UT (characterized by the transition of  $V_{\perp E}$  from eastward to westward velocities) and nighttime Harang discontinuities at 02 UT (identified by the southward  $V_{\perp N}$  velocity) are clearly defined. Using linear regression analysis on the  $V_{\perp N}$  and  $V_{\perp E}$  velocities, the distributions indicate

differences that are not so apparent when using only the averaged data (Figure 1 c and d). The distribution of the differences between velocities measured by the two techniques show that the DGS generally measured a lower velocity than that observed by the ISR, with a mean difference of 31m/s and a standard deviation of 91m/s for the  $V_{\perp N}$  component, while for the  $V_{\perp E}$  component the mean difference was 48m/s with a standard deviation of 120m/s. Taking into consideration the velocity uncertainties of each instrument and that the velocity amplitudes observed at Sondre Stromfjord are at times large (i.e. around 600 m/s), mean differences of less than 50 m/s are not significant. Hence, the velocities measured by both instruments are in good agreement, suggesting that generally at high latitudes the apparent velocity is a good measure of the plasma motion.

Scali et al. [1995] discussed the reasons for differences in the two velocities which occurred occasionally, particularly when the station was located near reversal boundaries in the plasma flow. Their analysis concluded that the main cause for these differences was the assumption of spatial and temporal uniformity made by the DGS and ISR techniques in the velocity calculation. While the high sampling rate of the Digisonde (5.12 sec) does not require the assumption of temporal uniformity, the ISR requiring approximately 17 minutes for one 3D velocity measurement is susceptible to violation of this assumption. In case of spatial nonuniformity the velocities derived by the DGS and ISR differ and either one is questionable. These studies indicated that a new method for extracting velocities from complex motions was needed. This led to the implementation of a method that had originated at UMLCAR some time ago, and is discussed in the following section.

### **3.1.3 The Generalized Digisonde Drift Analysis (GDDA): Measuring the Full Velocity Field.**

As discussed in the previous section, most techniques which calculate vector velocities make the assumption that the plasma motion is spatially uniform within the sampled volume. Due to the restrictions in the methods themselves, some instruments (i.e. such as the ISR where a velocity vector is calculated every 15 minutes when data from three well separated source regions are available) also need to invoke the assumption of temporal uniformity. While the Digisonde Drift Analysis (DDA) method does not need to assume temporal uniformity, the technique does rely on the assumption of spatial uniformity.

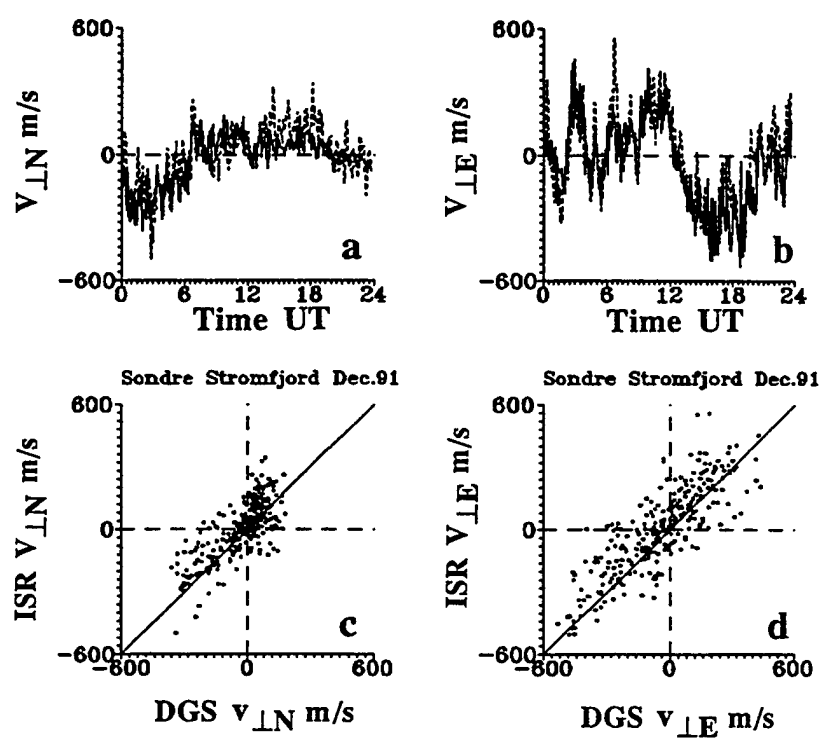


Figure 1. Five-day average of the  $v_{\perp N}$  and  $v_{\perp E}$  velocities and linear regression scatter plot (ISR, dashed line; DGS, solid line).



The investigations presented by Scali et al. [1995] of high latitude convection indicated that the motion of plasma within the sampled volume determined by the sounder may not be uniform. The Digisonde drift method must account for this in order to correctly identify the main velocity components within the volume. Since the Digisonde drift method is one of the few techniques that obtains a large number of reflection sources within a relatively short time, combinational analysis can be used to develop a velocity field distribution in which the main velocity components within a sampled region are resolved. The concept of the Generalized Digisonde Drift Analysis scheme (GDDA) is as follows: from a set of  $N$  sources, a subset of  $r$  is selected at a time to calculate a velocity, the total number of possible combinations is  $N!/[r!(N-r)!]$ . All combinations containing sources from the same plasma motion produce similar velocities, while combinations of sources from different plasma motions result in random velocities. The resultant distribution of velocities maps out a velocity field where the highest occurrence of specific velocities represent the velocities within the sampled volume.

The GDDA discussed here was developed at UMLCAR using DDA as the basic platform on which to construct a more generalized velocity calculation package. In this way, since DDA and GDDA share a certain intersection of common knowledge, proper interpretation of the results from one method genuinely enhances the understanding of the other method. Since GDDA uses combinational analysis, the number of velocities calculated for inclusion in the velocity field distribution is much larger than the number of sources detected. Table 6 gives an indication of the number of velocities that are calculated with GDDA as compared to DDA. As an example, for a drift subcase where 20 sources have been detected, if we calculate a velocity using combinations of 5 sources, previously with DDA only 16 velocities would be calculated, while with GDDA the possible combinations are 15,504. Since at high latitude stations like Sondre Stromfjord 20 sources per subcase is common, the GDDA method gives an enormous advantage in determining the velocity field more precisely. With these larger statistical samples, sources that have large errors associated with them produce low probability of occurrence peaks in the velocity field.

With GDDA it is still possible to group a number of subcases together for velocity calculations (as was previously available in DDA), and this further increases the number combinations. An example is given in Table 7 where for a group of four subcases (a subcase represents a single frequency, range, polarization bin, and four of these represent one case), 61 sources are obtained and using combinations of 4 sources at a time the total possible number of velocities calculated are 521,855. The last column in this table shows the number of velocities retained in the final velocity field (i.e. 15,324) after GDDA has filtered out velocities that do not meet certain criteria set up in

the GDDA menu. These criteria have been revised as the effects of the combinational analysis were better understood.

There are some disadvantages to the GDDA method, the biggest is that the computer processing time is increased. More combinations means more calculations. Table 8 offers some benchmarks.

**Table 6. DDA/GDDA Table of Possible Combinations**

No of Sources N =	DDA			GDDA		
	r=3	r=4	r=5	r=3	r=4	r=5
3	1	--	--	1	--	--
4	2	1	--	4	1	--
5	3	2	1	10	5	1
6	4	3	2	20	15	6
7	5	4	3	35	35	21
8	6	5	4	56	70	56
9	7	6	5	84	126	126
10	8	7	6	120	210	252
11	9	8	7	165	330	462
12	10	9	8	220	495	792
13	11	10	9	286	715	1287
14	12	11	10	364	1001	2002
15	13	12	11	455	1365	3003
16	14	13	12	560	1820	4368
17	15	14	13	680	2380	6188
18	16	15	14	816	3060	8568
19	17	16	15	969	3876	11628
20	18	17	16	1140	4845	15504

**Table 7. Testing Data Size; System Performance Table**

System	Data Group	No of Sources Averaged Over One Case	No of Possible Combinations Selecting 4 Srcs	Average No of Actual Combinations Used
DDAV	Subcase	15	12	10
GDDAV	Subcase	15	1365	56
DDAV	Case	61	58	54
GDDAV	Case	61	521855	15324

**Table 8. Processing Time Table**

Data Group	DDA Seconds	GDDA ( in Seconds )			
		GDDAV Format		DDAV Format	
		Ram-Drive	H-Drive	Ram-Drive	H-Drive
Subcase	0.22	1.96	2.88	1.73	2.64
Case	0.44	Insufficient memory > 3MB	850.46	No of Vel.s larger than internal arrays > 2000	No of Vel.s larger than internal arrays > 2000

Table 8 indicates the overall time taken for DDA and GDDA to process a subcase or a case of skymap data. GDDA has four columns which represent different processing and platform runs. When GDDA calculates the combinational velocities but handles the results with the DDA statistical packages, this processing is labeled DDA Format. GDDA also has its own statistical package, and processing test benchmarks are given under the GDDA Format column. GDDA does not rely on internal fixed size data arrays as was used by DDA. The intermediate results are written to temporary files. This has the advantage that GDDA is not restricted to a maximum of 2000 velocity points as was DDA. The amount of velocities that GDDA can now handle is only restricted by the size of the RAM or hard disk used for storage. Hence, benchmarks are given when GDDA uses the RAM or hard drive to store temporary files.

It takes DDA 0.22 seconds to process a subcase and 0.44 seconds to process a case of skymap data. GDDA takes a maximum of 2.88 seconds (for GDDA format, using the hard drive for temporary storage) to process a subcase, and 850 seconds for processing a case of skymap data. Even in its fastest mode for processing subcases, GDDA is at least 10 times slower than DDA. In its present configuration, this scheme can only be used in a post-processing environment.

The combinational analysis used by GDDA to obtain a velocity field was tested and refined for a known velocity component. Drift data were simulated for a resultant velocity with a vertical component of 10 m/s, a horizontal component magnitude of 100 m/s, and an azimuthal direction for the horizontal velocity component of 90 degrees (compass East). Three velocities were generated in the skymap for this one subcase of the simulated data. The three regions are well separated in zenith and azimuth to better optimize the velocity calculation. All sources were grouped around the original three region positions given as:

	Region 1	Region 2	Region 3
Zenith : Deg.	5	30	20
Azimuth : Deg.	30	150	270

The simulation was done for the antenna setup at Millstone Hill, that is for a seven antenna system, at a frequency of 4.0 MHz and group range of 220 km. A random number generator was used to provide a noise background. It is important to note that for each individual source, at least three Doppler lines associated with an individual source were identified as separate sources. This proliferation in the number of sources is a result of the Hanning weighting applied across the data set. Removal of this redundancy would decrease the processing time by reducing the number of sources and, consequently, the possible combinational number of velocities.

Running GDDA on this simulated data set, the velocity distribution of  $V_z$  had a median value at 10 m/s, the  $V_{ns}$  distribution has a median at 0 m/s and the  $V_{ew}$  distribution has a median at 100 m/s indicating that the GDDA program had correctly identified the known velocity components. However, the GDDA velocity distribution also peaks at a number of spurious velocities that do not correspond to the velocity inputs. These additional apparent velocities reduce the probability of occurrence for the true velocity. If the number of combinations is increased, as in the realtime environment, there will be occasions when the velocity field has many spurious velocities and the true velocity components will be absorbed in a wide box-like distribution. In situations where two velocities exist in the same sampling volume, these spurious velocities can make the task of separating the two velocities difficult. The question is where do these extra velocities come from.

Figure 2 displays the Horizontal Components of the Velocity Field (HCVF) for three separate runs as well as diagrams that can be used to better understand the source of these extra velocity components. The HCVF plots represents a plot of the horizontal velocity component north-south " $V_{ns}$ " plotted against the horizontal east-west component " $V_{ew}$ ". Below the HCVF plots is a diagram illustrating, with three small circles, the general position of the original three source regions simulated in the skymap data. In each circle are the number of sources GDDAV can use to calculate a velocity. For the original run (Figure 2a) all combinations were allowed, hence some of the 3982 combinations calculated individual velocities using three sources from the same region. Restricting GDDAV to only using at most "two" sources from the same location as was done in the second run produces a cleaner velocity field as shown in Figure 2b. The number of velocities accepted by GDDAV has now dropped to 3717.

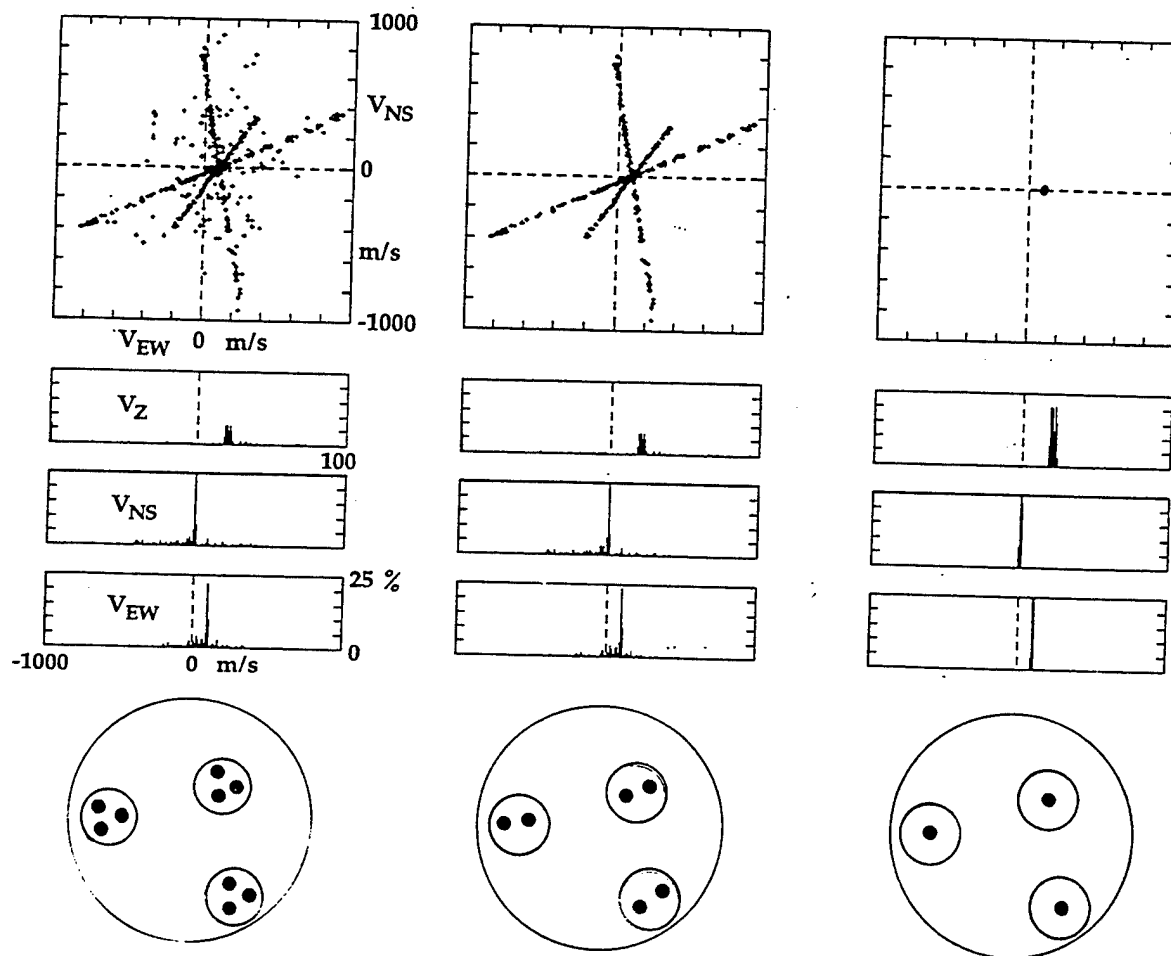


Figure 2. Horizontal Components of the Velocity Field (HCVF) plots for three separate runs as well as diagrams that can be used to better understand the source of these extra velocity components.

The most spurious velocity components have been removed, and all that remains are unique lines that represent the velocity calculated from the combination of two sources from the same region and one from another region. The intersection of these lines is naturally the true velocity. Going a step further and making GDDAV calculate velocities for those well separated sources, (i.e. only one source per region/circle) removes all of these extra velocities. Figure 2c shows the final result and now GDDAV only accepted 1152 velocities. The outcome is a set of sharp distributions representing the original known velocity. The solution is then to set criteria so that GDDAV only calculates velocities from a combination of sources that are well separated. Further testing indicated that for the best results only sources separated by at least  $4^\circ$  should be combined. DDA had in the past also suffered from this problem. Previously DDA velocity data always had some examples when the velocities vary dramatically from case to case. These simulations helped in the understanding of GDDAV.

Having refined the combination analysis used in GDDAV for a one velocity component, tests for two velocities in the same sampling volume were performed by splitting the sampling volume into two sectors. The first sector is represented by four sources located in zenith, azimuth coordinates at (25, 0), (25, 50), (25, 100) and (25, 150). In this sector the velocity was kept constant with components given as  $V_z = -15\text{m/s}$ ,  $V_h = 100\text{m/s}$ , and  $Az = 0$  degrees. The second sector is represented by the four sources located at (20, 200), (20, 250), (20, 300) and (20, 350). In this sector the horizontal velocity direction was changed for each run as shown in Table 9.

**Table 9. Horizontal Velocity Direction**

Run Number	Vz m/s	Vh m/s	Az degrees
1	-15	100	0
2	-15	100	30
3	-15	100	60
4	-15	100	90
5	-15	100	120
6	-15	100	150
7	-15	100	180

For each simulated run, 8 subcases were produced. The actual simulated velocity values for each run and the GDDAV statistically significant calculated velocities are given in Table 10. The 8 subcases, the run numbers corresponding to the velocity configuration given in Table 9 are shown. As the velocity of the second set of sources is rotated in azimuth, two velocity fields are observed. From run 1 to 4 there is a clear two component separation in the  $V_{ew}$  and  $V_{ns}$  velocity fields which give the correct magnitudes of these velocity components.

**Table 10. List of simulated known velocities in two sectors of skymaps and calculated main velocity components in each section using GDDA methods.**

Run	Simulated					GDDAV Calculated				
	Vz	Vns		Vew		Vz	Vns		Vew	
		S1	S2	S1	S2		S1	S2	S1	S2
1	-15	100	100.0	0.0	0.0	-15	100	100.0	0.0	0.0
2	-15	100	86.6	0.0	50.0	-15	100	86.0	0.0	50.0
3	-15	100	50.0	0.0	86.6	-12	100	50.0	0.0	86.6
4	-15	100	0.0	0.0	100.0	-20	--	0.0	0.0	100.0
5	-15	100	-50.0	0.0	86.6	-15	100	--	0.0	--
6	-15	100	-86.6	0.0	50.0	-13	100	-86.0	0.0	120.0
7	-15	100	-100.0	0.0	0	-25	--	-100.0	10.0	-25.0

A blank in Table 10 indicates that the frequency of occurrence for this velocity component is statistically insignificant. The results in this table show that for the first 3 runs, GDDAV correctly determined the velocity components for each individual sector. However, in this simulation GDDAV is unable to clearly identify the two velocity components, when their angular difference is greater than  $90^\circ$ , as is shown from the results of runs 4, 5, 6 and 7. This problem arises when the sources from different velocities have similar Doppler shifts. Given a specified field for the source locations (as shown in Table 9) and the two velocity components, the program SKYT.EXE was used to generate the drift data and write it out to a file in the typical Digisonde drift format. The drift data were processed to produce skymaps from which GDDAV determined the velocity field. Dependent on the magnitude and direction of the two velocities, two sources produce the same Doppler and the corresponding spectral line contains a composite signal. The resultant skymaps, therefore, display source locations that are not representative of the original source locations. In all cases, at least one velocity component from the velocity field is correctly determined. Run 5 correctly identifies the sector 1 velocity as  $V_{ns}=100\text{m/s}$  and  $V_{ew} = 0\text{m/s}$ , but does not find the velocity in the other sector. Run 6 reproduced the velocity in sector 1 correctly, but found a wrong speed for section 2. Usually the correct velocity has the largest frequency of occurrence, however, this is not always the case.

The solution to this problem was to devise an iterative procedure that extracts those sources that contributed to the velocity with the highest frequency of occurrence. The sources that are left are then used by GDDAV to calculate another velocity field. The idea behind this method is that if a second velocity is present, it should be observable from the sources that remain. Preliminary analysis has shown that this method is promising.

The GDDA technique was then applied to real data and the results showed the true power of the method in comparison to the previous DDA method. Figure 3, comparing the velocities calculated

with GDDA and DDA under exactly the same source selection criteria, illustrates the improvements attained in using the GDDA method. The data set used was from Sondrestrom for 19 June 1993. In this figure, three different time periods are shown with increasing complexity in the velocity field. Each plot shows ten consecutive velocities obtained from sequences of 5-second measurements. In Figure 3 the GDDA velocities are shown as black dots. At 2.28 UT, when only one velocity is observed, GDDA and DDA are in good agreement, well within the error bars. As more velocities occurred in the field-of-view (at times 16.28 and 5.28 UT) the DDA median velocities differ considerably from the GDDA values. The GDDA median velocity remains consistent, while the DDA velocity changes drastically from measurement-to-measurement; the DDA  $V_{ns}$  and  $V_z$  components generally show the largest deviations from the GDDA values.

Figure 4 shows the results of applying GDDA to Sondrestrom drift measurements from 8 December 1991 for two different local magnetic times, (a) 12 CGLT and (b) 22 CGLT. The cartoon on the left side shows the location of Sondrestrom at these two times relative to a two cell convection pattern. At 12 CGLT, (Figure 4a), CDA identifies a single velocity, signaling uniform velocity with the Digisonde's field-of-view. At 22 CGLT (Figure 4b), GDDA detects two velocities suggesting that Sondrestrom is at the edge of the Harang discontinuity. Both eastward (250 m/s) and westward (600 m/s) flow existed within the field-of-view.

From the GDDA results obtained so far, it is estimated that nonuniform velocity fields exist about 50% of the time at high latitudes. Consistent use of GDDA for the analysis of Digisonde drift data is therefore mandatory for the high latitude stations.



# GDDA (circle)/DDA(square) comparison Sondrestrom 19 June 1993

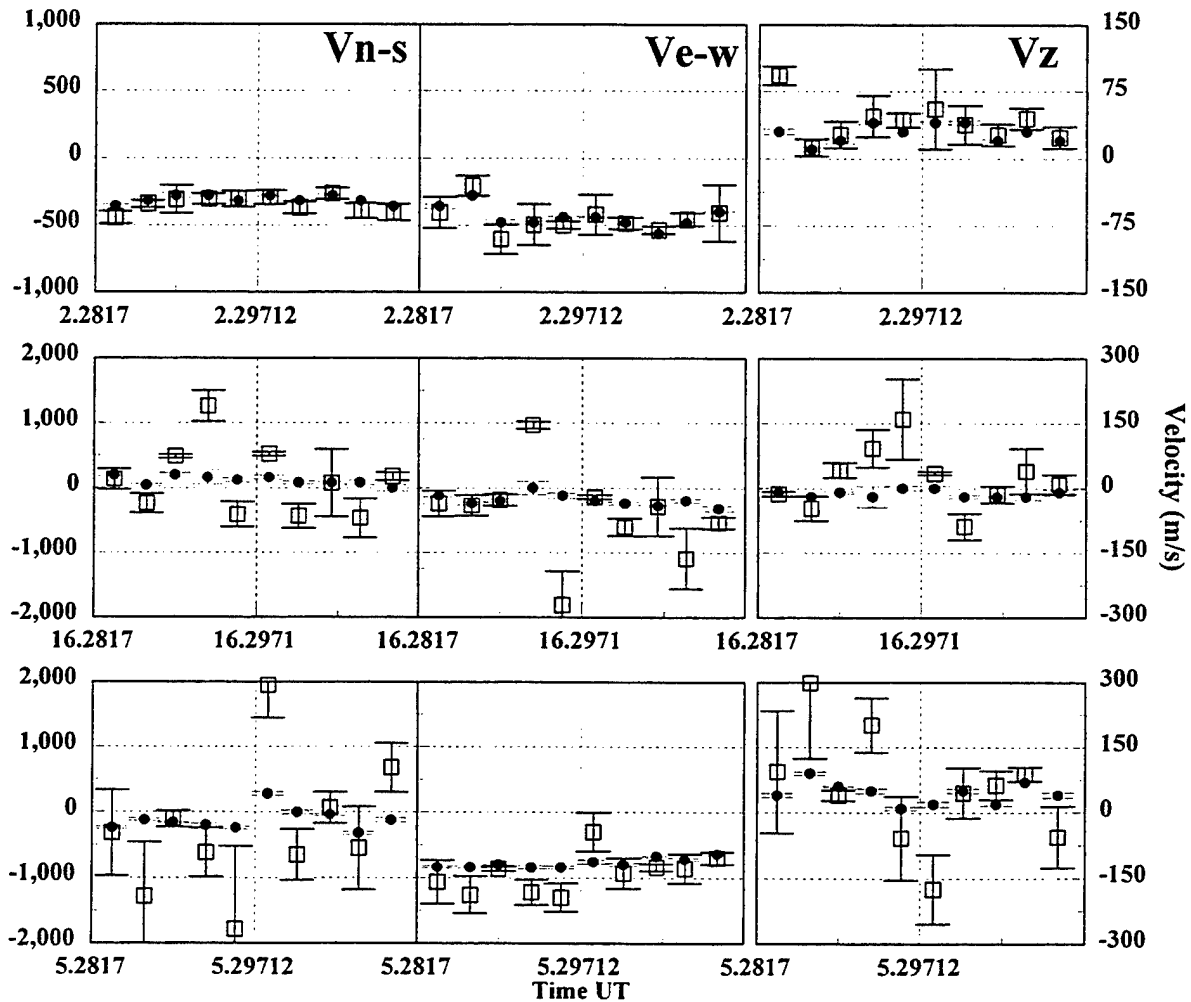


Figure 3. Comparisons of the median velocities calculated from GDDA and DDA under exactly the same source selection criteria, illustrating many of the improvements attained in using the GDDA method.

# GDDA : single and multiple velocity distributions.

## Sondrestrom 8 December 1991

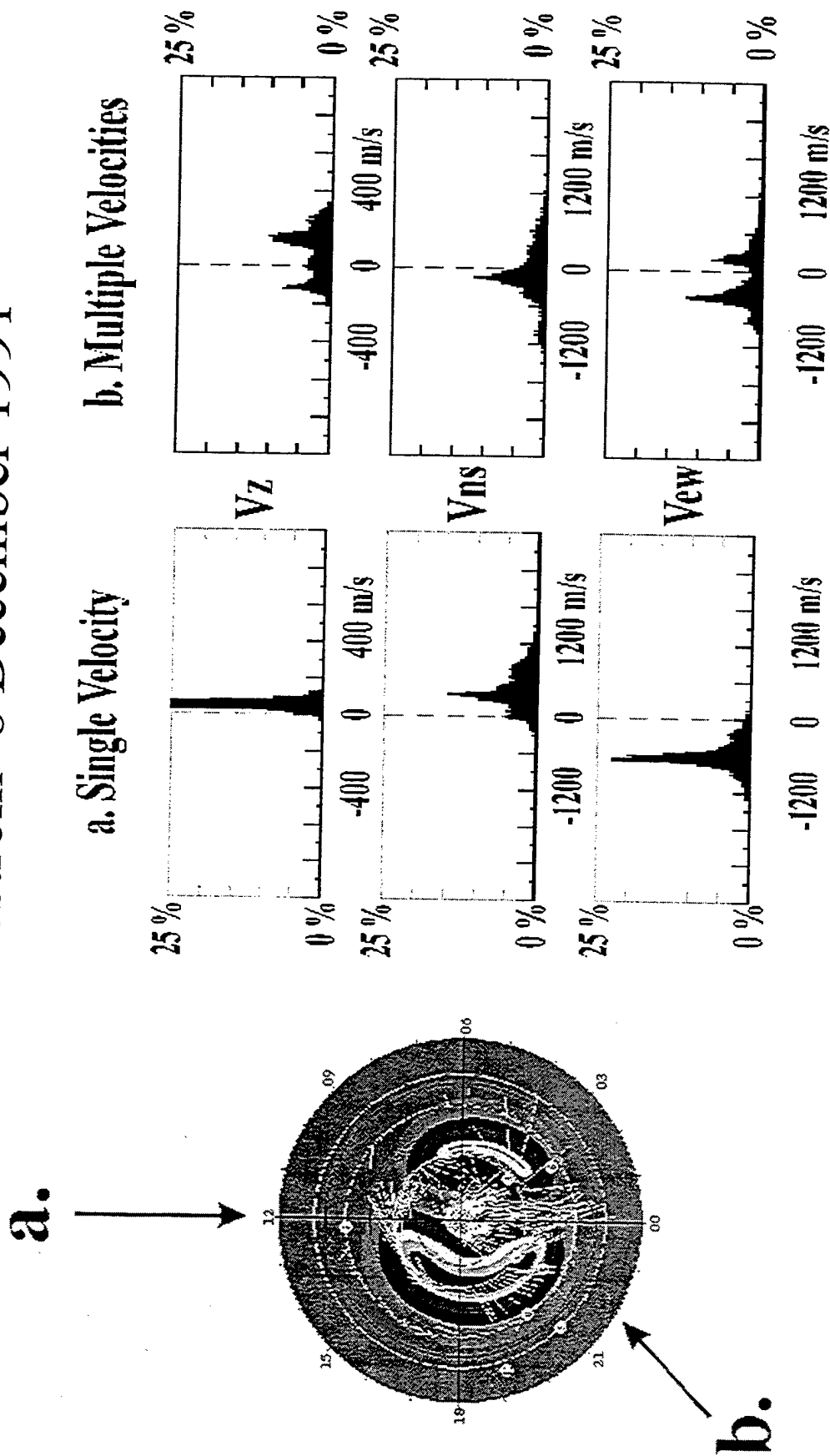


Figure 4. An example of the GDDA distributions for the case when a single, and multiple velocity is detected in the field of view.

#### **3.1.4 Determination of the IMF Bz and By Orientations from Digisonde Drift Data**

Empirical and mathematical models exist that map the polar convection patterns. To specify the convection pattern the models require, as a minimum, inputs for the orientation of the IMF (sign of Bz and By), and the position of the dayside cusp region. The direction of the IMF directly influences the structure of the polar circulation patterns and must be known. It was concluded that the process could be reversed and the direction of the IMF be determined from the circulation pattern.

From data obtained at Qaanaaq (Greenland) over a three-year period, (1989-1991) a statistical analysis for the behavior of the plasma motion under different IMF conditions was done. Correlating known IMF orientations with Digisonde velocities measured during these years, criteria have been developed that related variations in velocity to the signs of Bz and By. Using these criteria and allocating confidence weights it was possible to determine the sign of the IMF Bz and By components from the Digisonde drift velocities. The method devised to determine the signs of Bz and By from measurements at one station (Qaanaaq) proved to be 60 to 70% reliable. In order to improve these estimates various factors had to be considered. These were:

(1) Because at certain time periods different IMF results in the same drift velocities, this method should be tested only when the station is located at CGLT sectors where changes in the convection patterns are clearly defined by different Bz and By conditions.

(2) Introduce other stations in the determination scheme. Stations such as Sondre Stromfjord and Svalbard which rotate through the cusp region can contribute to the overall improvement of the IMF determination especially for the By component.

To improve the determination of the IMF Bz and By components from Digisonde velocities, a detailed statistical analysis similar to that done for Qaanaaq was needed for other stations. This analysis would help to interpret convection pattern signatures at latitudes other than Qaanaaq which can be used to infer the orientation of the IMF. A reasonably complete Digisonde drift data set for Qaanaaq, Sondrestrom, and Svalbard exists for the year 1993 (data set for Svalbard only covers period from January to July 1993).

Digisonde drift data collected at Svalbard from January to July of 1993 have been processed and monthly medians were extracted for comparison with the Sondre Stromfjord monthly median

velocities. The monthly median vertical " $V_z$ ", horizontal north-south " $V_{ns}$ ", and horizontal East-west " $V_{ew}$ " velocities have been calculated. Sondrestrom experienced hardware difficulties during the month of February 1993 and only two days of questionable Digisonde drift measurements were obtained during the entire month. Little weight should be placed on these data.

The results of this analysis show that the Sondre Stromfjord vertical monthly median velocities for the summer months have well-defined diurnal characteristics in comparison with the diurnal variation as seen at Svalbard. At times they differ considerably. The two stations are comparable in geomagnetic latitude, however they differ in geographic latitude by about 10 degrees. At Sondre Stromfjord, during the summer months, the apparent vertical velocity shows the characteristic chemistry control of the ionosphere. The effect of increased photo-ionization is observed as negative velocities at sunrise (around 6 UT) which gradually decrease in magnitude until local noon (i.e. 15 UT) when  $V_z$  is approximately zero. In the afternoon and evening hours a positive increasing  $V_z$  component is observed. Svalbard does not show any of the solar control observed at Sondre Stromfjord.

During the winter months, Svalbard displays strong southward  $V_{ns}$  velocities in the afternoon, dusk sectors. The characteristics of this velocity component differs considerably from the overall diurnal variation recorded at Sondre Stromfjord. Differences are also observed in the  $V_{ew}$  component. The geomagnetic similarities and geographic differences makes the Svalbard and Sondrestrom stations ideal for mapping out the convection patterns in two distinct locations in the two-cell structure where both stations transverse the cusp region at different times.

Statistical analysis methods were developed to assess whether the average drift diurnal variations are significant in light of the daily variability that is often observed. Previous analysis showed monthly medians with large daily variability due to changing IMF conditions. By testing the means of the monthly distributions in an independence test, it is possible to see if changes over different months are significant when the daily variability is larger than some of the diurnal variations observed in the monthly median data sets. The tests were carried out on the 2 sigma significance level, hence a probability of 1.0 indicates that the two data sets, at the 95% level of certainty, are independent. A low probability indicates that the two data sets are not sufficiently dissimilar in characteristics when considering the daily variability observed throughout the month.

The test for independence for the three velocity components,  $V_z$ ,  $V_{ns}$  and  $V_{ew}$  was carried out. The months compared are January and July 1993 for data sets collected at Sondre Stromfjord. The most noticeable high probability levels are observed from 01 to 06 and from 16 to 23 UT for the

View velocity component. At these times changes observed in the monthly medians are significant in spite of the daily variability. Hence, these changes signify seasonal differences in the monthly median data that are real and not associated with the daily variability. In the case of the  $V_{ns}$  component, the only times that significant changes are observed are from 03 to 09 and from 15 to 18 UT. The significance of these changes are smaller displaying maximum probability confidence of 0.88 as compared 1.0 for the View component. The vertical component  $V_z$  displays the most significant differences around 01 to 03 UT and 6 to 12 UT. The daytime differences in the apparent vertical velocity component  $V_z$  are real and are associated with the chemistry control of the ionospheric layers during the northern hemisphere summer months.

This dataset can be used with confidence to determine the seasonal changes in the drift velocities observed at Sondrestrom and make it possible to design a set of criteria to reproduce the monthly median velocities observed at the station. The set of criteria obtained from the statistical comparison of the Sondrestrom daily velocities with IMF orientations, can now be implemented in PCM determination of IMF orientations relying on drift information from two Digisonde stations.

### **3.1.5 F-region Polar Cap Convection Pattern**

Using drift data from Qaanaaq, Sondre Stromfjord and Goose Bay for 14 and 15 January 1993, potential patterns and recalculated velocity vectors were produced using an in-house program based on the Heelis [Heelis et al., 1982] model concept. The position of the ten high latitude Digisonde stations that are, or have been, in operation in the last few years were considered in determining the circulation pattern. As a means of accessing if any measurable event took place within the sampling period, each potential circulation pattern was determined after introducing another 3 hours of drift data. For example, the potential patterns obtained at 15 UT, 18 UT, 21 UT and 00 UT on 15 January 1993 are determined successively (Figure 5 displays the potential patterns calculated for 00 and 18 UT).

In comparing potential patterns calculated at 15 and 18 UT, the results obtained indicate that at the 18 UT, the dawn (dusk) cell showed an increase (decrease) in potential from 17.27 kv (-31.4) to 20.9 kv (-42.44). After this time, the dawn (dusk) potentials decrease (increase) gradually. While this program facilitates the interpretation of the measured velocities at different locations in terms of variations of two cell patterns, it is still limited to the original Heelis two-cell pattern and offers very little flexibility in reproducing an actual convection pattern, which may be much more complicated. Hence, other more developed models, such as the Heppner-Maynard [1987] and

advanced Heelis [private communication, 1982] models were collected and looked into as a platform for the Polar Cap Monitor (PCM) recognition system.

To enhance this analysis, data from the Defense Meteorological Satellite Program (DMSP) were collected and in-house programs setup to manipulate this data set for inclusion into the pattern recognition system. The DMSP satellite data form the primary data set from which convection patterns can be constructed. The Digisonde drift database provides support to this data set and maintain continuous coverage for times when the DMSP satellites are not located over the northern hemisphere polar region. The DMSP data set selected for preliminary testing were recorded on day 342, 1991 by the F8 and F9 satellites.

The vertical and horizontal (orthogonal to the satellite path) velocities as well as the geographic latitude and longitude position of the F8 and F9 DMSP satellites were available. The time period covered is from 14 to 15 UT on day 342, 1991. The event of interest in this period is around 1430 UT when the IMF Bz component went from strong southward to a strong northward orientation. At Sondre Stromfjord, the ISR measured a large northward velocity of 1300 m/s. Both satellites show similar behavior in their measured horizontal component, i.e. an increased negative velocity up to a maximum of 1000 m/s. Table 11 gives the geographic coordinates of the satellites and Sondre Stromfjord at this time.

**Table 11. Geographic Coordinate Matrix**

Satellite/ Station	Geographic Latitude	Geographic Longitude
	Degrees	Degrees
F8	75 N	80 E
F9	60 N	270 E
Sondre Stromfjord	67 N	310 E

Even though at 1430 UT the satellites and ISR are well separated in latitude and longitude, the observed switching of the IMF Bz sign is affecting both measurements indicating a large scale change in the polar convection pattern. This event is a good example of why a real time potential pattern recognition scheme is essential. Within minutes significant changes in the entire polar convection were observed. The convection model is still being developed; however, the results obtained indicate the importance of the PCM initiative in supplying realtime convection patterns as the basic input for any model [Scali, 1992].

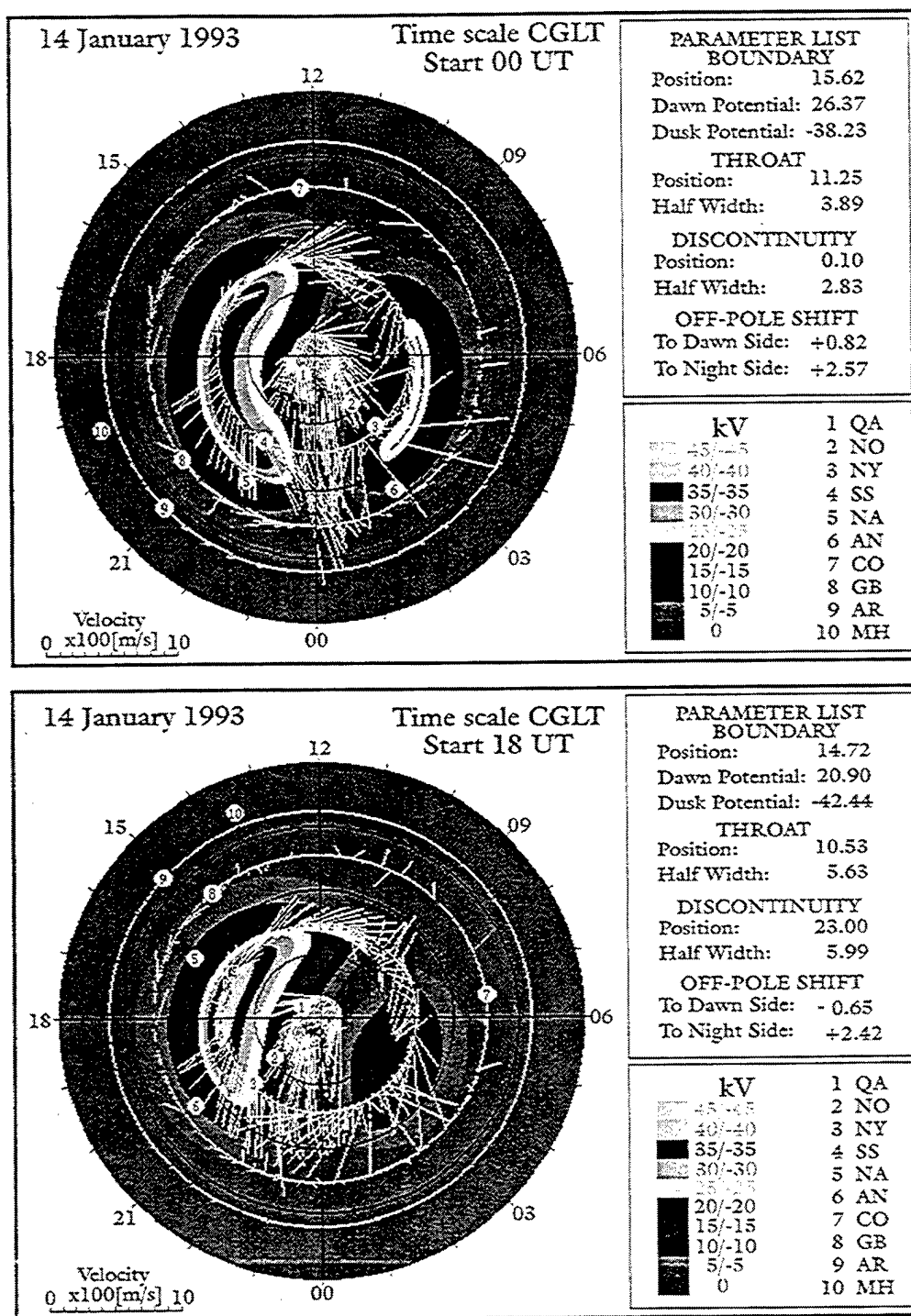


Figure 5. Potential patterns calculated for 00 and 18 UT.

### 3.2 Mid-latitude Trough Studies During Geomagnetic Active Periods

Digisonde measurements at Millstone Hill, Goose Bay, and Qaanaaq during storm time conditions were analyzed to determine the characteristics of the midlatitude trough during geomagnetically active periods. For three main storm events in March 1990, June 1991, and November 1993, the following analysis was performed: scaling of ionospheric parameters, calculation of true height electron density profiles, calculation of the horizontal velocity magnitude "Vh", the azimuthal direction of the horizontal component "az", and the vertical component "Vz". The results of these investigations indicate that [Scali et. al., 1997]:

- a) As geomagnetic activity increases the F layer moves to higher altitudes and the electron densities decrease, resulting in the formation of trough regions;
- b) There is an increased speed of the horizontal drift in the direction opposite to the rotation of the earth;
- c) Higher latitudes are more sensitive to minor changes in the geomagnetic activity in comparison to lower latitudes;
- d) The mid-latitude trough expands equatorwards with increased magnetic activity;
- e) Daytime upper F-region is affected more than the E and lower F regions during geomagnetic storm times.
- f) When geomagnetic activity increases, convection velocities at high latitudes increase.
- g) The G-condition ( $foF2 \leq foF1$ ) does not occur with all geomagnetic storms. This condition is observed in the June 1991 storm but is not seen in the March 1990 storm.
- h) The Digisonde results for several storms within the same month show that the recovery stage in the ionosphere is dependent on the intensity of the geomagnetic disturbance in the main phase of the storm.



### 3.3 Equatorial Depletion Bands

As part of the Phillips Laboratory/MISETA equatorial campaign, UMLCAR analyzed drift and ionogram data from Jicamarca (Peru) and Agua Verde (Chile). Standard processing resulted in the isodensity contours for foF2 and hmF2 recorded on 30 September, 1 and 2 October 1994 including the FF and QF indices, parameters that identify the amount of frequency and range spread present in the ionogram.

On 30 September, range and frequency spreading are observed from 0015 to 0300 UT. On the next night (1 Oct. 1994) no spreading was observed, and hmF2 from 00 to 01 UT was approximately 40 km lower in altitude than the previous night. Spread F was observed from 23 to 00 UT, and as on 30 September the height of the F-region peak was well above 300 km. The sequence of spread and no-spread F days offers the ability to investigate differences in the state of the ionosphere that could help identify those processes responsible for the generation of spread F. In these examples, the results indicate that the crucial time for the generation of spread F irregularities is between 00 and 01 UT (19 and 20 LT). When the height of the F-layer peak was below 300km during this time, no spread F event was observed. However, when the height of the F-region peak was above 300 km at this time, spread F was likely to be observed at Agua Verde and Jicamarca.

On nights when spread F was observed in the ionograms, large altitude oscillations of the ionospheric layers occurred. At Aqua Verde, the altitude variations occurred before and after the onset of spread F. In nights without spread F, the height of the F-region did not show this behavior. Comparison with the Jicamarca data set shows a similar behavior, however differences do exist.

An examination of the Agua Verde Digisonde data indicated the occurrence of strong spread F on two of the nights, in particular, days 94-274 and 94-276. Comparing the times of occurrence of the spread F with the all-sky 6300A images it was difficult to determine the relationship between the location of the depletion bands and the spread F on the ionograms. To resolve this situation we developed a simple electron density model of the depletion band and then used 3-D ray tracing to investigate how these depletions are perceived by the HF radio waves. It became immediately apparent that these HF signals easily became trapped within the depletion, making it possible to achieve orthogonalities with the field-aligned electron density irregularities within the depletion walls. These multiple simulations showed that the spread F was present as long as any depletion was within about 300 km of the sounder site, consistent with the observations.

On the basis of this work a paper was prepared for presentation at the International Symposium on Equatorial Aeronomy, held in Bali, Indonesia. This paper included the simulated sky maps generated using our model of the equatorial electron density depletion and our 3-D ray tracing code. Here, the azimuth and elevation of the incident rays were plotted for each ray that encountered an orthogonality with the earth's magnetic field within the walls of the depletion region. The depletion region was made to drift eastward by moving the sounder station for each set of ray tracings. Scattering of the HF signal was observed in the walls of the depletion regions somewhat south of the station at Agua Verde. This southward shift occurs because of the magnetic dip at these locations, favors orthogonality to the south of the sounder. The general character of the simulated sky maps was very similar to the actual sky maps. The poster paper raised some interest for our new techniques of modeling ionospheric structures. A second paper was prepared for the Ionospheric Modification Workshop held in Santa Fe, NM. Here, we introduced the concept of ionospheric "imaging" for any disturbed region of the ionosphere, in particular, the heated regions produced by a high power HF transmitter such as at Arecibo or HAARP in Alaska.

The drift and ionogram data at Jicamarca (Peru) and Agua Verde (Chile) that were recorded as part of the MISETA/Phillips Laboratory equatorial campaign, show significant differences in the ionospheric characteristics during spread F events observed at these two equatorial stations. While spread F events are often observed at both stations on the same nights, the irregularities and their generation mechanisms may not be the same. For example, when spread F occurred at 0429 UT on 28 September 1994 at both stations, at Agua Verde much more diffuse spread F structures were observed than at Jicamarca. At Agua Verde, extended F-layer spread F traces display similar characteristics to the slant-F features observed at higher latitudes, i.e., scatter beyond the F layer critical frequency. Considering the similarities, this suggests that this type of spread F results from small-scale field-aligned irregularities. The spread F signatures at Jicamarca, on the other hand, suggest the presence of much larger scale irregularities. The difference could purely be due to the orientation of the reflection/scattering irregularities at each station. Considering the dip of the magnetic field lines at Agua Verde, reflections are more common from the south of the station. At Jicamarca where the dip is essentially zero, east and west reflections are predominately observed during spread F conditions.

The results obtained from this analysis indicate that a prerequisite for the development of spread F irregularities is that the F-layer is at a high altitude around 19 LT. The lifting of the layer from the normal diurnal variation is caused by induced electric fields. On no spread F nights the rise and fall of the F layers at the two stations appear to be anticorrelated in the time around 19 to 23 LT. The F layer at Agua Verde begins to move up when the F layer at Jicamarca falls. This behavior is not

associated with the movement of the terminator since sunset at Agua Verde is earlier than at Jicamarca. This behavior indicates a linkage in the dynamics controlling the ionosphere at both stations.

The height rises due to the effect of electric fields are apparent on spread F nights. Typically, at around 19 and 22 LT similar height variations occurred at Jicamarca and Agua Verde with a slight time delay. Jicamarca observed the effects of these electric-fields almost one-half hour before they are observed at Agua Verde. This time difference is compatible with the separation of these two stations in longitude, and the event propagating from west to east. The effects of this event were intense spread F which persisted throughout most of the night until sunrise. The event observed at 1930 LT in the night of 9/30 to 10/01 are similar but smaller, since the "normal" height variation at the two stations was still observed. Spread F on this night lasted only from 19 to 22 LT.

Using the Silicon Graphics work station at Phillips Laboratory the measured Digisonde skymap data were overlaid on the all-sky images of the depletion bands at Agua Verde. Although the images at 630.0 nm were available every minute, the Digisonde produced a skymap at a particular frequency, say 3 MHz, only once every 10 minutes. This analysis produced the important result that the dominant location of the skymap sources lay within the depletion bands and that they moved along with the depletions as they drifted eastward. This confirms that the spread F on ionograms and the clustering and locations of skymap sources are the same phenomenon originating from medium-scale electron density irregularities within the depletion band. This multi-instrument observation of the F region disturbances confirmed that the Digisonde, operating in the drift mode, can image and track the depletions during their east-west passage over the station, supporting the optical observations (Sales et al., 1996).

### **3.4 Geophysical Multi-Instrument Visualization**

The UML Institute for Visualization in collaboration with UMLCAR scientists developed and implemented under the direction of Ron Pickett a basic visualization system to present in 3-D structures and events within the ionosphere. Specifically, the Agua Verde data from October 1994 were presented with new display software. The Institute for Visualization and Perception Research at University of Massachusetts Lowell has constructed this package for Phillips Laboratory using IBM's Data Explorer program.

J.L. Scali had suggested the introduction of the IBM visualization program because of its more user friendly environment in comparison, for example, to AVS. Data Explorer is a second

generation visualization application and tool kit, which provides users with a means of applying advanced visualization and analysis techniques to gain insights from simulations, observations, and models, in any combinations. This ability to combine different data sets and perform visual correlative analysis gives the users unique capabilities. Data Explorer employs a data flow client/server execution model with the capability to distribute visualization across multiple workstations in a heterogeneous environment.

During the early assessment stage, UMLCAR scientists were able to load the DX Data Explorer software on the Hanscom Phillips Laboratory's SGI computers, and run prestructured modules for the visualization of a number of geophysical data sets. Using their predefined networks, the Digisonde drift data were coded within the DX explorer environment and rendered in a visual environment. Skymap data obtained at Agua Verde on 1 October 1994 were plotted on the world map, and Data Explorer has the capability to zoom in on this map for observing the data close up as it would appear from a satellite view of the South American coast.

Once the Skymap data set was input into Data Explorer, color mapping, coordinate transformations, surface rendering, data tagging, zooming controls, axis labels, rotation of axis options are all available in the DX environment. This assessment of the package and communications with the IBM Data Explorer personnel indicated that this visualization software would be very attractive. At the time of this report, both Phillips Laboratory and the Institute of Visualization and Perception Research have implemented Data Explorer.

#### **4. Digital Oblique Remote Ionospheric Sensing**

Oblique swept frequency sounding over relatively long radio paths has been for a long time an important part of HF communications management. A new application of this sounding technique involves remote sensing of the ionosphere when a vertical incidence sounder is not convenient or possible at a particular location. The DORIS project was an attempt to demonstrate the utility of the Digisonde for this application. A path from Wallops Island, VA to Goose Bay, Labrador was selected as an ideal oblique link, a convenient distance of about 1200 km and a path that had vertical sounders at both ends and near the midpath, that is at Millstone Hill Observatory, Westford, MA and Bangor, ME.

The major difficulty with using oblique sounding to determine the local (midpoint) ionosphere in real time is the need to automatically scale and then to invert the oblique ionogram into a vertical electron density profile. The automatic scaling technique requires the recognition on the oblique

ionogram of the several traces associated with E- and F-layer propagation and to differentiate between ordinary and extraordinary polarization modes. The DORIS project was aimed at implementing these requirements so that standard oblique ionograms from the Digisonde could provide a remote sensing capability [Kuklinski et al., 1992; Reinisch et al., 1992].

The approach to accomplishing this task required:

1. Actual oblique ionograms over the specified path to be used for processing with the auto-scaler and then with a direct inversion algorithm that uses either one or two quasiparabolic layers to represent the midpoint electron density profile.
2. Then based on comparisons between the predicted and measured midpoint electron density profiles a modified inversion algorithm would be developed that allowed accurate and efficient operation.

For the first phase of the project, a set of oblique ionograms from Wallops Island to Goose Bay were made along with a set of simultaneous vertical ionograms from the Maine OTH radar site near Bangor that would be used to evaluate the one/two layer direct inversion algorithm. Using the oblique ionogram processing technique, an equivalent vertical midpoint ionogram is calculated from the midpoint electron density profile that was derived using the oblique inversion algorithm. Then, this equivalent vertical ionogram is compared to the actual vertical midpoint ionogram recorded at the Maine OTH radar site. In all cases, consisting of 25 data sets, the inversion algorithm produced electron density profiles with critical frequencies within 200 kHz, and peak heights within 20 km of the measured values.

When the simulated annealing optimization inversion algorithm was used, a majority of the quasiparabolic electron density profiles showed a bias or offset between the oblique ionograms produced via ray tracing through these electron density profiles and the corresponding actual oblique ionograms. Although the simulated annealing optimization eventually corrected these errors a more efficient approach was also developed for this problem. In the improved inversion algorithm several observed propagation mode extremes would have to be satisfied before the final simulated annealing optimization technique is applied. The three observed propagation mode conditions that the midpoint quasiparabolic electron density was forced to satisfy are:

1. A least one low-angle ray reaches the known ground range at the lowest observed low-ray sounding frequency.

2. No ray reaches the known ground range for any frequencies above the observed MUF frequency.
3. At least one high-ray reaches the known ground range at the lowest observed high-angle ray sounding frequency.

When these observed propagation mode extreme conditions are satisfied, which can be accomplished in an efficient manner, the final adjustment of the quasiparabolic model parameters necessary to satisfy the observed group path conditions is then accomplished using the simulated annealing optimization technique.

#### **4.1 Network Synchronization**

Prior to this project, UMLCAR had updated the DISS system at Wallops Island, Virginia as well as the Digisonde 256 located at Millstone Hill, Massachusetts with hardware modifications for automatic network synchronization using the GOES satellite as a reference. During July 1991, two UMLCAR personnel traveled to the DISS site at Goose Bay to install the synchronization modification. Upon completion of the hardware modification, an oblique link was established between Goose Bay and Wallops Island with Wallops Island synchronized via telephone. To accomplish this synchronization several problems had to be addressed with the GOES satellite. These included:

- The East satellite was considered temporary. The East GOES satellite was not in the position expected by the GOES receiver thus the receiver always indicated a position error. Moreover, the GOES time from the East satellite showed a diurnal variation of  $\pm 4.7$  milliseconds compared to our Rubidium stabilized time reference.
- The GOES receivers used at Millstone and Goose Bay had to be switched to either East or West satellite but not left in Automatic Satellite selection mode. In automatic, there was a 20 millisecond uncertainty depending on which satellite is automatically selected.
- Even with careful antenna positioning the West satellite, viewed from Goose Bay, is on the horizon and was receivable only during the evening and night.
- A recommendation was to use a relatively inexpensive Hy-Gain amateur radio 432 MHz Yagi antenna, which was superior in performance to the existing Kinometrics antenna at Goose Bay.

- The West satellite appeared to have a  $\pm 0.5$  millisecond variation on the scale of hours. Obviously for any sort of operational DORIS a more reliable GPS time synchronization system was necessary.

## 4.2 Algorithm Development

The development of the DORIS algorithm required two major tasks:

1. A two-stage inversion algorithm, one that iteratively adjusts the quasiparabolic layer parameters first to satisfy the observed propagation mode extreme before applying the simulated annealing optimization technique, was implemented and used to process the Wallops Island to Goose Bay oblique ionogram database.
2. The electron density profile model used by both the direct and two-stage inversion algorithms was extended to include up to three complete quasiparabolic layers.

The two-stage inversion algorithm was implemented by the addition of an iterative procedure that in sequence 1) adjusted the base height of the layer until at least one low-angle ray reached the known ground range at the lowest observed low-angle ray sounding frequency; 2) adjusted the critical frequency of the layer until no ray reached the known ground range for any frequencies above the observed MUF frequency and 3) adjusted the semi-thickness of the layer until at least one high-angle ray reached the known ground range at the lowest observed high-angle ray sounding frequency. This sequence of adjustments was repeated until all three of the observed propagation mode extremes were satisfied simultaneously.

The preliminary "coarse" inversion process was tested using the Wallops Island to Goose Bay oblique ionograms. In every case, the procedure converged in less than 100 iterations (30-45 seconds of processing time on an Apollo 3500 work station) to a quasiparabolic layer model that produced group paths at all recorded sounding frequencies that were within 50 km of the actual group paths. The subsequent simulated annealing optimization algorithm made "fine" adjustments in the layer parameters resulting in electron density profiles with critical frequencies within 200 kHz and peak heights within 20 km of the measured values.

The electron density profile model used by both the direct and two-stage inversion algorithms was modified to include up to three complete quasiparabolic layers. A preliminary evaluation of both the direct and two-stage inversion processes using this three layer model indicated that an additional

modification of the electron density profile model would be required to produce adequate results for a wide range of ionospheric conditions. The major limitation of the present electron density profile model is the assumption that each layer is a complete, separate quasi-parabola. This simplifies the mathematical analysis since the determination of the E-layer parameters establishes a limit of the base height of the F1 layer, for example. An adequate electron density model for a wide range of conditions must allow for layers that are segments of quasi-parabolas. This requires modification of the group path calculation portion of the inversion algorithms and the development of code to determine the intersection heights of these quasiparabolic segments.

The electron density profile model was modified to allow the quasi-parabolic layers that represent each layer to intersect the others. The intersection heights were determined from the critical frequency, base height, and semi-thickness of each layer and used as limits for the appropriate integrations required to determine the group path and ground range of a ray of known takeoff angle. An additional necessary modification of the automatic processing program was the addition of a code to identify each ray as being a high- or low-angle ray. This is done by evaluating the derivative of the ground range with respect to the takeoff angle for each ray. The ability to analytically identify each ray as being a high or low ray increased the speed of the simulated annealing algorithm.

The entire DORIS software package was transferred from the Apollo work station to a 386 based computer system. This allowed the real-time operational characteristics of the entire DORIS software package to be evaluated as it might perform in the field. One additional modification of the present software package was to implement a noise cleaning and echo trace enhancement filter using a spatial domain convolution operation rather than a frequency domain filter that requires the computation of the two-dimensional Fourier transform of the oblique ionogram and the inverse two-dimensional Fourier transform of the resulting product of the filter transfer function and the ionogram transform.

The three-layer quasi-parabolic electron density profile ray tracing algorithm that included full echo and high/low ray identification has been implemented and tested. After successful validation, the algorithm was modified, using the derivative of the ground range with respect to the takeoff angle to determine ray divergence, that made it possible to calculate the relative power of each ray. This ray tracing and homing algorithm were combined to produce a reliable software package capable of generating synthetic oblique ionograms for any link where the ionosphere at the reflection point was known [Huang et al., 1996].



The Goose Bay to Wallops Island oblique ionograms were compared with synthetic oblique ionograms, generated using a midpoint electron density profile derived from the scaled Maine OTH vertical ionograms. The comparison of these ionograms indicated that in many cases the two-hop propagation modes was an important feature of the oblique ionograms and must ultimately be made part of the inversion process. To accomplish this, the synthetic oblique ionogram software was modified to include calculation of the two-hop propagation modes. This required the assumption that the ionosphere was identical at each of the three reflection points involved in multi-hop propagation. The relative power of both the one- and two-hop modes are also calculated.

## **5. Joint Electronics Warfare Center Project**

This project, in support of the Joint Electronics Warfare Center (JEWEC), represents the efforts of Ron Brent of the Mathematics Department of the University of Massachusetts Lowell.

This research effort was directed towards the modification of the 3-D ray tracing program HARPO-HC to include Gaussian Beam intensity calculations. JEWEC was provided with a new 3-D code capable of solving complicated propagation problems consisting of the transmission of an EM wave in the atmosphere with irregular terrain and refraction profiles. The code they used was based on ray theory and hence, suffered from the inadequacies arising when using a geometrical optics approach - namely, difficulties with the appearance of caustics (and the solution nearby) and with the existence of shadow zones.

JEWEC was advised that the best method for dealing with these deficiencies is by using a Gaussian Beam approach. Typically, ray tracing programs compute the rays (or normals to surfaces of constant phase) connecting a source point to a receiver point and their associated travel time (or phase). By examining a ray bundle surrounding the receiver it is possible to calculate the spreading loss or amplitude of the ray. By summing, either coherently or incoherently, all the complex contributions of each individual ray connecting the source to the receiver one obtains the intensity. Problems are encountered when using this technique in the vicinity of caustic regions. When a ray passes through a caustic, there is a shift in phase, therefore, for coherent intensity calculations one must know the location of all the caustics and to determine whether or not a ray has passed through one. This is a difficult and time-consuming process. Solutions near a caustic are theoretically infinite (although not physically reasonable) hence, one must also correct for this problem. There are also regions through which no rays pass, so-called shadow zones, and the method predicts no propagation (also not physically reasonable). An additional numerical problem associated with ray theory is the determination of the so-called eigenrays.

When using a Gaussian or geometric beam approach, most of the preceding problems are removed. The basic idea behind a beam approach is to surround the rays with tubes in which the full wave equation is solved (either numerically or analytically). Key parameters in using this method are the beam curvature and half-width. Variables associated with the beam are the arc length,  $s$ , (proportional to travel time) and the normal distance,  $n$ , from the center of the beam or the ray. The wave equation in the  $(s,n)$  system is approximated by a parabolic equation which can be easily matched to obtain the solution. The solution of the parabolic equation is reduced to solving a first order system of equations for the quantities  $p(s)$  and  $q(s)$ . These two functions give the beam curvature and half-width. Phase is still determined by travel time but now corrections for passing through caustics are easy to apply. Passing through a caustic causes a sign change in  $q(s)$  and one can easily check for this when integrating for  $q(s)$  and correct immediately. There is no need to determine the actual location of caustics, or find out when the beam has crossed the caustic. Exponentially decaying solutions are obtained in shadow zones since these regions are "covered" by the beams. The problem of theoretically infinite solutions near caustics, however, still remains. Finally, since intensity calculations only require beams near the receiver, there is no need for an eigenray determination. One must be sure that the receiver locations are well covered by beams.

The question of the numerical technique for solving the problem with the beam approach was the next consideration. Since the core of a beam tracing routine is in fact a ray trace program, the numerical techniques used in finding rays determines the techniques for finding beams. Currently, there are two main approaches to calculating rays. The first method is to divide the region up into triangular sectors in which the light speed is fit by a linear function. Rays in a linear velocity field are circular arcs. By connecting the analytically obtained arcs one can determine a ray. The problem with this method is the appearance of false caustics due to the unphysical discontinuity between triangular regions. The advantage is that it is computationally very fast. The current ray trace core HARPO, uses an integral approach whereby the ray equations are actually integrated over the velocity field. This requires continuously differentiable models for functions such as light speed and terrain profiles. This way there are no false caustics, however, one incurs slower run times. The auxiliary equations for  $p(s)$  and  $q(s)$  can also be solved in these two ways. The existing 2-D beam code "BELLHOP" uses the first technique. One may also find analytical solutions for  $p$ , and  $q$ , if the velocity field is linear. We used the second technique since that is the way HARPO runs. The equations for  $p$  and  $q$ , are integrated numerically.

This technique involves a 3-D formulation of the equations for  $p$  and  $q$  in a spherical coordinate system. Numerical algorithms were developed for the solution of the first-order system of equations, and then we implemented this algorithm in the existing HARPO code.

To deal with high frequency long range anomalous EM propagation in realistic environments, the 3-D ray trace HARPO code based on Hamiltonian equations in spherical coordinates has been selected, adapted, and used. As a ray trace program it is subject to the singularities associated with caustic generation. In order to: 1) avoid the complications of identifying caustics and correcting associated errors, and 2) lower the frequency regime for which the method is applicable, a second theory using beams was sought. The assumptions and derivation of beam equations from initial wave equations is elaborated upon later in this summary; however, the underlying theory for beams uses ray tracing. The beam approach, or Gaussian beams, has greater accuracy near shadow zones and caustics, and is computationally more efficient than ray theory as stated earlier. The reasons for computational efficiency is that one does not need to locate caustics in order to make corrections, nor does one have to specifically find the eigenrays connecting the source to the receiver. This cuts down computational time dramatically.

Based on the work of Cerveny, Popov, and Psencik, an existing 2-D beam program developed in ray centered coordinates was obtained and used. However, the real need is to establish a 3-D beam program that uses the excellent ray trace of HARPO while accounting for variable terrain as well as earth curvature. The problems associated with this approach are listed below:

1. The delivered 2-D Gaussian beam code BELLHOP, cannot be modified to include terrain in a simple manner. By simple, we mean the incorporation of terrain effects through a modified index of refraction. Solution of 2-D problems using BELLHOP would require a complete rewrite of the program. Such efforts would be better spent on the adaptation of HARPO to include Gaussian beams.
2. While the code HARPO is in a spherical coordinate system (thus naturally accounting for earth curvature) existing 3-D beam equations are derived in Cartesian coordinates. This leads to two possibilities. Either: a) we have to re-derive the 3-D beam equations in spherical coordinates or, b) we calculate the rays in spherical coordinates then superimpose them on a Cartesian system in which the beam equations are numerically integrated. It was learned that doing (a) is far too difficult, and that (b) is the correct way to proceed. Reasons are given below.
3. The benchmark code FOR3D, a 3-D implicit finite-difference parabolic approximation using a fourth-order Douglas solver, has been obtained. There were several system-based changes that have had to be made before the code is usable. This is the most accurate 3-D PE code

available, and it comes with analytical solution benchmarks which we used to test the final 3-D Gaussian beam code.

For brevity, details of various analyses and results are not included. The initial thrust of efforts were reviewed and corrected the analysis of Ryan to see if this could be used in some way to modify the analysis for the 2-D beam development so as to account for earth curvature and variable terrain. Efforts were also placed on establishing compatibility between beam equations and the spherical coordinate structure of HARPO. In this effort, all the wave equations of Ryan were re-derived and in a number of cases corrections were made.

The method of Gaussian beams began by rewriting the scalar wave equation using a ray-based orthogonal curvilinear coordinate system. What allows the mathematics to be carried out in the theoretical derivation of the beam equations is the fact that one does not need the actual ray paths, but only the associated ray-based system metrics. In Cervený and Hron, a complete derivation of ray-based system metric is given relative to a Cartesian system. These equations are coordinate system independent, in the sense that the Laplacian can be written down knowing the system metrics. Even if the actual coordinate system is not known, one can rewrite this equation using the appropriate metrics. One could carry out similar mathematical arguments and derive modified beam equations including effectively the earth's curvature, but not variable terrain.

Consequently, wave equations that are transformed from spherical coordinates to Cartesian coordinates with horizontal boundaries via such earth flattening methods with variable terrain were not usable as a starting point for a beam equation derivation. In order to use "BELLHOP", one would have to modify the code to include terrain input data, and then calculate the rays and beam parameters incorporating terrain reflections and losses. This is not a trivial matter, and it was decided that efforts would be better placed on deriving 3-D beam equations and implementing a 3-D beam program using HARPO, which already has terrain effects built in.

A review of the pertinent derivations of the kinematic ray trace equations with and without Hamiltonians was carried out. A 3-D formulation using cylindrical coordinates only, suggested by Porter and Bucker [1987], was questioned and found not applicable. A 3-D extension of the beam equations in ray-centered coordinates referenced to Cartesian coordinates can be obtained from the 3-D beam equations in elastic inhomogeneous media by Cervený and Psencik [1983] and Cervený [1985].

One possibility was to use a modified height to incorporate terrain and earth curvature as a boundary with respect to a Cartesian system by which the ray-centered beam equations are related to the rays without using a spherical coordinate ray trace solution such as HARPO. This would involve the complete programming of a Cartesian based HARPO-like ray trace. To obtain the sophistication and robustness of HARPO, this would be too difficult. The second approach, previously shown to be not possible, was to incorporate terrain and curvature as a modified Helmholtz equation, and derive beam equations referenced to Cartesian coordinates. Then by first calculating the rays with HARPO in spherical coordinates, one could translate these ray coordinates into Cartesian and integrate the modified beam equations along the rays. Not only was this found to be impossible, but it is numerically inefficient. Efficiency dictates that the beam equations be solved concurrently with the ray tracing algorithm. This approach required fewer file reads and writes.

The next approach was to try to establish the ray-centered beam equations with respect to the earth-centered spherical coordinate system. At the time we believed that this was the only way one could directly use HARPO. This would avoid the conversion of rays from spherical to Cartesian coordinates. Establishing the beams relative to a spherical coordinate system turned out not to be usable. The characteristics (system of partial differential equations) of the eikonal equation giving the rays were derived in spherical coordinates. From these equations the rays are determined and the basis vectors of the ray are expressed in a ray-centered coordinate system with respect to spherical coordinates. Further, the ray-trace Hamiltonian equations in spherical coordinates were derived. The detailed analysis of Cerveny and Hron on the 3-D metrics of the ray-centered system was studied in hopes of generalizing the results to ray coordinate systems based relative to spherical coordinates. Part of the method needed the Frenet equations from differential geometry. These equations relate the tangent, normal and bi-normal vectors of a curve. To continue this line of investigation we needed to determine the Frenet equations in spherical coordinates. We were able to use the concept of intrinsic derivatives to mimic their arguments and derive metric tensors. Unfortunately, the complicated forms of these metrics are not suited for use in the determination of the beam equations. This was an unfortunate dead end, but it shed light on the entire theory of the ray-based coordinate system, and led to the final usable approach.

Finally, we arrived at the most direct approach. One calculates the rays using HARPO, in spherical coordinates, and simply overlays the rays on a Cartesian system on which the beam equations are integrated. As it turns out this is most sensible, since the beam equations are only dependent on arc length, which is coordinate system independent. Other functions in the beam equations can be simply evaluated at appropriate points along the ray. The variable terrain is already incorporated

into the ray tracing, and one could also incorporate the variable terrain into the beam equations. We now discuss the derivation of 3-D beam equations in Cartesian coordinates.

The derivation of 3-D beam equations for elastic wave propagation has been carried out by beginning with a Cartesian wave equation in 3 dimensions. Our needs are not in elastic propagation, which is a vector-field problem, but simple 3-D scalar propagation; however, the derivation can be easily adapted to our purposes.

By beginning with Maxwell's equations and assuming symmetry in one coordinate direction, it is possible to split the vector problem into two scalar problems, corresponding to vertical and horizontal polarization. These scalar problems were then solved using parabolic approximation techniques. Typical numerical techniques used to solve the parabolic equation are implicit finite difference schemes (IFD) and the split-step Fourier transform technique. These techniques were used to make the differential operator discrete, that is to say they are microscopic methods.

Limitations of these methods are in that the grid mesh over which the solution is computed must be small enough to yield accuracy. This often means grid sizes are on the scale of three wavelengths. At high frequencies and long propagation ranges this could amount to millions of points needed for solution. A better method to solve the equations is by symbolically integrating the equation with respect to range thereby obtaining the macroscopic propagator. In theory, if one does a good enough job at approximating the macroscopic propagator it is possible to take very large range steps. The macroscopic operator is approximated using a Pade rational function series. The more terms used in the approximation, the larger the steps one can take. For  $n = 8$ , one can take range steps on the order of 10 to 100 wavelengths. For  $n = 40$ , one can take steps on the order of 1000 wavelengths. This cuts down the computational problem significantly. Another advantage of this method is that the operator may be applied in parallel. That is, each of the 'n' Pade approximations may be applied to the field at the same time as opposed to having to apply a series of operators sequentially. For cases when the desired result is the loss values near the receiver, and not at many points in-between the source and receiver, the Pade technique applied to the macroscopic operator is perfect. It cuts down the number of intermediate range locations at which the field must be computed.

An acoustic code exists that can be run on a parallel processing machine. It has been shown that this code converges to solutions with run-times on the order of 1/100 to 1/1000 that of ordinary IFD's or Split-Step Fourier transform methods. We have acquired the code, and modified it for use in electromagnetic problems. To do so, the theory for scalar propagation models has been

examined. Corrections for conservation of energy have also been derived. This handles the problem of vertical interfaces at the terrain boundary for cases when the slope is non-zero. That is the problem of staircase approximations to sloping terrain. When parabolic approximations are applied to range dependent problems, the method of implementation is to model the medium as a series of range independent sectors.

When modeling the terrain elevation this means continuously sloping terrains are given as a series of staircase-like structures. At each step in the staircase there is an artificial vertical discontinuity. Since the parabolic approximations can satisfy at most one condition in range, typically taken to be continuity of field, we asked the question whether or not this is the best method. It was felt that a better condition to apply is conservation of energy. To do so, one first begins with the physical theory to decide what quantity is conserved. For our case it turns out that the electric or magnetic field should be scaled by the inverse square root of light speed. In implementing this new dependent variable, at each step where continuity of field is applied, one automatically conserves energy. The work now focused on the conversion of the acoustics program EFEPE, to the electromagnetic situation. The EM code is named SSP. This code is a split step Pade solution to the parabolic approximation for EM propagation. The code uses a macroscopic operator representation for the solution, with subsequent rational function approximations. The acoustic code was remodeled to accept EM inputs and the problem was solved with excellent accuracy. This problem is one where an EM source is placed between two perfectly reflecting plates. A simple analytical solution is available for comparison.

The completion of the code SSP as well as the delivery of two post-processing graphics routines GRAPH2 and GRAPH3 was our main effort. These graphics programs gives the user the ability to display screen contour plots of intensity losses. The completion of SSP included the implementation of matching conditions at the earth-atmosphere interface using the concepts of virtual points. Many tests were run to see how the implementation worked. Since no analytical models were available for EM situations, the method of virtual points was tested in an acoustic case using known solutions. The method was shown to work quite well.

This material was presented to the JEWG. The code SSP was actively commented, and final user friendly versions delivered to the JEWG. Efforts to find EM analytical models to test the interface conditions were also carried out, to no avail. The code SSP was demonstrated including the graphics routines.

## **6. Digisonde Network Support**

For the entire duration of this contract, in support of the USAF programs, we have helped maintain and support the DISS network as well as other sounders that were operated in support of Phillips Laboratory research efforts. This included the sounding systems aboard the Airborne Ionospheric Observatory also operated by Phillips Laboratory. The UMLCAR effort is presented in chronological order as the most logical approach detailing the five year effort. Small details that had been discussed in the Quarterly Reports are left out of this Final Report.

### **6.1 April - July 1990**

#### **6.1.1 Bermuda Naval Air Station (NAS)**

The site was visited during 9-12 May 1990 to correct malfunctions and perform a system calibration. Several technical modifications were carried out. After correcting malfunctions in Frequency Synthesis and Automatic Gain Control/Frequency Search operation, a calibration of the receive antenna performance indicated the antenna field is in excellent condition. Reflected signals at 9 MHz are consistently lower in comparison with 8 and 10 MHz though transmit antenna power input is nearly constant. The transmit antenna probably has a minimum in the vertical radiation pattern in this frequency region. Installation of a small vertical rhombic and associated antenna switching was suggested to improve this situation if the problem is considered serious enough to warrant the expense.

#### **6.1.2 Argentina Naval Air Station (NAS)**

A Final Power Amplifier (FPA) malfunction occurred during May 1990 which rippled through other elements of the transmitter portion of the DISS resulting in component failures. The problem was diagnosed and corrected by telephone with the technician at the site. A vacuum tube failure in the FPA originated the fault. On 24 May 1990 replacement parts were sent to GL to be forwarded to Argentina. A set of FPA tubes should be provided to the site as soon as possible. During July 1990 UMLCAR visited the site to calibrate system performance, provide maintenance and install applicable updates.



### **6.1.3 Goose Bay, Labrador**

During late July 1990 UMLCAR installed and tested recently developed receiving antennas at Goose Bay with the goal of improving performance at higher frequencies and finding a solution to the echo directionality problem. The DISS configured printed circuit boards that were removed for the purpose of implementing updates were left on-site without any configuration changes performed on them. All improvements to this site were accomplished by inserting modified cards provided by UMLCAR.

### **6.1.4 Airborne Ionospheric Observatory (AIO)**

The AIO was currently undergoing periodic depot maintenance with all project equipment removed and held at Pease AFB and Hanscom AFB/GL for re-installation during September 1990. UMLCAR planned to provide technical support during the re-installation including system calibration in preparation for the upcoming OTH test mission including onboard operation.

During the reporting period, technical support has been provided to GL in the form of consultation and direct effort concerning quality control of equipment re-installation and providing of on-board maintenance supplies to support forthcoming AIO missions. This effort continued in mid-August 1990 to bench-check performance of the digital ionospheric sounding components of the AIO in preparation for the re-installation.

## **6.2 August - October 1990**

### **6.2.1 Argentia NAS**

The site was visited by UMLCAR personnel on 28 and 29 July 1990 to calibrate system performance and correct any deficiencies. Considerable effort was involved in repairing connectors and cables of the receive loop antenna system. The incidence of connector and cable failure due to corrosion in the sea air environment at this site is high. A silicone compound applied to all outdoor connectors earlier this year does not appear to have improved this situation. Another visit to this site was necessary to install more effective sealing of outdoor connectors and replace all the loop internal elements that suffered from corrosion deterioration.

### 6.2.2 Goose Bay, Labrador

D. Kitrosser and K. Bibl visited this site during July 1990 to install and test recently designed small loop receiving antennas and conduct oblique sounding tests with the Millstone Digisonde. A new version of some cards were installed in the Processor to provide O/X drift, close spaced frequencies in ionogram and drift, phase code, double range and fast mode Drift modes of operation. A new timing card was incorporated to provide GOES synchronization and synthesizer reset for automated oblique sounding operation.

Four new small-loop antennas were set-up on 80 meter baselines. The reduced effective height of these antennas results in reduced signal amplitude requiring an additional current amplifier. For the same reason, gain resistors in the Polarization Switch/Preamplifier boxes beneath the new small-loop antennas, have been changed from 300 to 50 ohms. Polarization recognition tests in vertical and oblique ionograms gave perfect results for all frequencies.

In the first attempt to synchronize with the Millstone site it was discovered the phase code was wrong because the Millstone GOES receiver offset was set to the wrong satellite. Considerable difficulty was experienced using GOES for synchronization. After much effort it was discovered that the East satellite is out of fuel and not in the position expected by the GOES receivers so a position error is always indicated. In addition, time from the East satellite showed a  $\pm 4.7$  millisecond diurnal variation relative to the site rubidium standard. The West satellite has a  $\pm 0.5$  millisecond variation on the scale of hours.

The new Precision Group Height Oblique Sounding mode was tested between Goose Bay and Millstone. While results are promising, the utility of this mode depends on the degree of "roughness" of the ionosphere.

The AWN modem and/or the dedicated line to Carswell AFB were not working much of the time UMLCAR personnel were present at Goose Bay. Although much effort was expended to keep the system operational for one-half hour and hourly ionograms, outages still occurred due to AWN modem/line problems. Newfoundland Telephone Co. replaced the AWN modem but Carswell and Global Weather Central still called frequently. It appears likely these problems were associated with the high temperatures that prevailed in the building during this unusual heat wave at Goose Bay.

The Uninterruptible Power Supply (UPS) often tripped off line and then went into oscillation. It appears that the UPS was overloaded having to power two tape recorders, two printers and all modems in addition to the ARTIST computer. The load was reduced by connecting some items directly to building (raw) power before leaving the site.

### **6.2.3 Airborne Ionospheric Observatory**

During the week of 24 September, UMLCAR personnel tested the airborne 128PS Digisonde system at Phillips Laboratory and participated in preparations to re-install project systems in the aircraft scheduled to commence 1 October 1991. UMLCAR provided engineering support during the re-installation/test phase at Pease AFB from 1 to 18 October and then participated in airborne missions supporting tests of the West Coast OTH radar system.

## **6.3 November - January 1991**

### **6.3.1 Bermuda NAS**

The Bermuda Digisonde displayed a series of problems during the reporting period. All maintenance actions were accomplished via telephone with the technician in Bermuda. The initial problem was that the ARTIST failed to scale all ionograms on a regular basis. First indications were that the hard disk may be defective. A replacement hard disk and set-up floppy disk were sent to Bermuda in December. The hard disk was replaced, however, the set-up disk was found to be defective after shipping. A complete replacement ARTIST was sent to Bermuda. Replacement of the ARTIST did not completely rectify the original problem. Disconnecting the tape drive from the ARTIST cleared the intermittent scaling problem. After continued evaluation the cause of the failure was determined to be the tape drive. After cleaning the tape drive heads and tape drive interconnecting cables the tape drive resumed normal operation.

### **6.3.2 Argentia NAS**

During December an on-site visit to the field site by UMLCAR engineers was conducted. The purpose of the visit was to conduct corrective maintenance to the system, transmit antenna and receive antenna array.

### **6.3.3 College Station, Alaska**

During the reporting period an on-site visit to the field site by an UMLCAR engineer was conducted in December. The purpose of the visit was to restore the DISS to its original

configuration and deploy Version 1.1 of the ARTIST software. In 1988 the DISS system had been approved for modification for use in backscatter experiments. These experiments have since been completed and the backscatter modifications were removed from the DISS system.

#### **6.3.4 Sacramento Air Logistics Command**

During the reporting period an on-site visit to the field site by an UMLCAR engineer was conducted in December. The purpose of the visit was to deploy Version 1.1 of the ARTIST software, provide software installation training to the depot personnel and to assist the software logistics personnel in answering technical questions.

#### **6.3.5 Goose Bay, Labrador**

During the reporting period an on-site visit to the field site by UMLCAR engineers was conducted in December. The purpose of the visit was to conduct corrective maintenance to the system and receive antenna array. During the last week in January we were informed that the power supply in the ARTIST computer had failed. At the conclusion of the reporting period preparations were being made to ship a replacement power supply to the field station.

### **6.4 February - April 1991**

#### **6.4.1 Bermuda NAS**

This site was visited on 25-26 April to diagnose and repair an intermittent fault in the Digisonde that had begun to occur more frequently. Prior to this visit many attempts were made to diagnose the fault by telephone with the technician at the site. These efforts did provide considerable information concerning the cause, but the intermittent nature of the fault, apparently in the receiver section of the Digisonde, made diagnosis difficult. Earlier in this period there had been problems in ARTIST components of the system which may have masked the first, infrequent occurrences of the receiver fault. By the time of this visit the ARTIST computer, Techmar card and Tape Recorder had all been replaced by units shipped from UMLCAR in late February and March.

The receiver fault was identified as a missing 32 MHz local oscillator signal in the Processor unit. Although the fault was clearly observed for nearly one hour while searching for the exact cause, the signal, with correct amplitude and frequency, suddenly appeared and Digisonde operation was restored. It is believed repeated removal and insertion of some of the cards may have cleared the problem since the fault could not be provoked and has not re-occurred.

#### **6.4.2 Argentia NAS**

At the beginning of the reporting period, the technician identified that the Pertec tape drive had failed. A replacement tape drive was shipped to the site via air cargo and the defective unit returned to UMLCAR for repair. At the close of this period, the technician at this site reported possible Final Power Amplifier, transmit antenna or transmit antenna cable/connector problems.

#### **6.4.3 Goose Bay, Labrador**

During the reporting period failure occurred in the IBM-PC/AT. In February, a replacement power supply was shipped to the site and installed by Balgit Gill. However, the fault was then traced to a faulty disk drive shorting the power supply. A replacement IBM-PC/AT was shipped to the site and the faulty unit returned to UMLCAR for repair.

#### **6.4.4 Airborne Ionospheric Observatory**

During February, the AIO was engaged in a continuation of the CRRES missions begun on January 7 and terminated at Pease AFB on 23 January. For the February segment, the AIO departed Pease AFB on 8 February 1991. R. Gowell (UMLCAR) was involved for a total of approximately two days of technical preparation and testing of AIO project systems at Hanscom AFB and Pease AFB prior to the 8 February departure from Pease AFB. J. Moore (UMLCAR) served as Mission Director on the AIO during the February missions. During the last of these flights staged from Sawyer AFB in Michigan, the airborne ionospheric power amplifier failed. Data of marginal quality were acquired by operating at greatly reduced power output. UMLCAR provided some assistance in diagnosing this problem by telephone on 17 February. Since this was the last flight of the mission, it was decided the aircraft should return to Wright-Patterson AFB and UMLCAR/Phillips Laboratory personnel would repair the failure there before June '91 CRRES missions commenced.

In March 1991, the airborne Digisonde 128PS system was delivered to UMLCAR by Phillips Laboratory for diagnoses and repair of apparent loss of receiver gain, increased ringing after the transmitter pulse and an intermittent condition, although infrequent, that totally disabled operation of the processor.

## **6.5 May - July 1991**

### **6.5.1 Bermuda NAS**

Follow-up action by telephone continues pertaining to previously reported visit in April when receiver malfunction was traced to a missing 32 MHz local oscillator signal. The fault disappeared suddenly while diagnosing the oscillator card. Mr. Mike Flynn, at the site, is monitoring system performance closely, but has not seen a re-occurrence of the fault. UPS battery is dead to the extent that the start-up problems occur after a power failure. The UPS has been removed and returned to UMLCAR.

### **6.5.2 Argentia NAS**

At the start of the reporting period the site technician reported arcing at the termination resistor mounts. The arcing was eliminated by installing tape insulation around the mounts.

### **6.5.3 Airborne Ionospheric Observatory**

During May 91, Robert Gowell of UMLCAR and SSgt. Twing of Phillips Laboratory traveled to Wright-Patterson AFB to perform maintenance on the airborne ionospheric sounding system in preparation for CRESS missions in July 91. Although the AIO would come to Pease AFB for mission staging, there was concern that diagnoses of an equipment failure that occurred during the February missions, might require long delivery replacement parts of excessive time to accomplish repairs. This action was later well justified when mission staging commenced in June.

During July, Robert Gowell traveled to Pease AFB to install and test the Digisonde 128PS system in the AIO and prepare project systems for the forthcoming missions. During three days effort an intermittent, defective cable and connector were found in the Granger 1128 Power Amplifier, apparently the original cause of the February failure and considerable damage in the Power Amplifier. With repairs completed, including replacement of all vacuum tubes in the Granger 1128, performance with the refurbished Digisonde 128PS was excellent. Although UMLCAR personnel did not participate in the missions, test procedures were reviewed with Phillips Laboratory personnel to enhance early detection of this type of failure in the future.

## **6.6 August - October 1991**

### **6.6.1 Bermuda NAS**

At the close of the reporting period, the Bermuda Digisonde 256 was reporting too few strobes along with the transmitter dropping off-line at the start of an ionogram and subsequently recovering later in the ionogram. A set of printed circuit cards were sent to Bermuda via express mail. Continued telephone evaluation of the transmitter resulted in learning that by running at a slower repetition rate the transmitter functioned throughout the entire ionogram. The system was fully operational while operating on the slow repetition rate. Evaluation of the faster repetition rate problem was postponed to the next reporting period.

### **6.6.2 Argentina NAS**

At the start of the reporting period the tape drive malfunctioned and the on-site rep was unable to clear the malfunction. A replacement tape drive was shipped to the site and the defective drive returned to UMLCAR.

During the latter part of the reporting period the system failed to operate off the hard disk in the ARTIST IBM-PC. The system was restored by operating off the executable floppy disk in disk drive A. A replacement disk controller card and hard disk were shipped to the station via parcel post.

## **6.7 November - January 1992**

### **6.7.1 Bermuda NAS**

At the start of the reporting period the processor repeatedly reported an error message "Too Few Strokes," however, the system continued to produce ionograms. By reducing the repetition rate of the transmitter from 200 Hz to 100 Hz cleared the error message. Replacement processor cards were sent to the site. These cards were received and installed into the system by the technician. The old cards that were removed from the system and were returned to UMLCAR. The system was fully operational on all repetition rates.

During the reporting period UMLCAR received three telephone calls from AFGWC identifying that data were not being received over the AWN. On each occasion the station was polled via the dial-up modem with confirmation that the Digisonde was operational. In each case, the on-site representative was contacted and asked to perform testing on the local network to confirm data

being placed on the AWN by the Digisonde. In all three cases the trouble was determined to be external to the island and that all data requirements of the Digisonde were fully operational.

#### **6.7.2    Argentina   NAS**

At the close of the previous reporting period the Digisonde was operating on the floppy disk drive due to a failure of the hard disk or disk controller. A replacement hard disk and a disk controller card were shipped to Argentina. At the start of this reporting period these items were installed in the system with the defective units returned to Lowell. The system was restored to a fully operational status.

#### **6.7.3    Qaanaaq, Greenland**

Due to the poor quality of communication lines between Thule, Greenland and Qaanaaq, Greenland, as well as the non-availability of a telephone satellite link between Lowell and Thule, we have been unable to poll the Digisonde 256 at Qaanaaq on a routine basis.

In December the contractor was notified that the Digisonde has suffered a failure in the processor core. The Digisonde was shutdown awaiting receipt of replacement cards.

#### **6.7.4    Narssarssuaq, Greenland**

During the reporting period the contractor was notified that the DISS transmitter had failed. This failure had been resident for a couple of months, however, due to the poor quality communication lines to the station the contractor was unable to routinely poll the station. Contact was made with the site representative, Mr. Soren Larsen at the close of the reporting period. Telephone communications were difficult to acquire and could only be accomplished after 1800 L.T.

### **6.8    February - April 1992**

#### **6.8.1    Bermuda   NAS**

At the close of the previous reporting period we had received multiple telephone calls from AFGWC regarding the non-availability of Digisonde data on the AWN. In all cases, verification was received from Bermuda that data were received up to the point where the lines leave Bermuda and that the cause of the failure was not resident in Bermuda. As a precautionary action a replacement interface card within the Digisonde that interfaces with the AWN modem was sent to the station and installed in the system. Reports from AFGWC of Digisonde data non-availability



were received on two additional occasions during the reporting period after the card replacement and as before verification of data availability was performed on the island.

During the second week of March the replacement tape drive was received via government shipping. This unit worked until the latter part of April when the tape drive began malfunctioning and causing the ARTIST to hang-up. The tape drive was disconnected from the ARTIST and connected to the Processor chassis. This scheme, at least, enabled the system to record the processor data. The tape drive troubleshooting continued into the next reporting period.

During the final week of the reporting period, the transmitter failed. The on-site representative visited the station and reported that the air conditioner unit had frozen causing the temperature within the trailer to increase, causing the transmitter to shutdown. On visual inspection of the transmitter, the four 4.7nF, 6kV capacitors on the Receiver Tap transformer in the Final Power Amplifier had disintegrated due to an electrical failure. Replacement capacitors were shipped to the station via Government channels.

#### **6.8.2    Argentina NAS**

At the start of the second month of the reporting period, the system was not producing ionograms when polled on the dial-up modem. Due to the severity of the weather the on-site technician was unable to gain access to the sounder for two weeks. Once on-site, the processor chassis was reset using the reset button on the front of the chassis. The system returned to operational status. The system was operational until the end of this month when the replacement on-site representative Mr. Chuck Pilcher called to inform us that the transmitter failed to transmit. After four days of telephone troubleshooting the two capacitors in the Final Power Amplifier (FPA) chassis and two resistors required replacement. Replacement of these components restored the system to a fully operational status. However, after approximately one week of operation the transmitter difficulties returned. At this time it was determined that the FPA chassis required replacement. A replacement chassis was available at the Phillips Laboratory and shipment to the station was initiated. The transmitter system was shutdown during the last week of the reporting period to await receipt of the replacement FPA.

#### **6.8.3    Qaanaaq, Greenland**

At the close of the previous reporting period UMLCAR was informed by Phillips Laboratory that the system had been shutdown due to a core failure in the processor chassis. Replacement cards were carried to Sondrestrom by Phillips Laboratory personnel and sent to Qaanaaq via mail. Mr.

Sven Eric found the defective card. The system was operational at the start of April 1992. At the start of the reporting period UMLCAR was able to establish telephone communications with the site. We have found that this link can only be established after 1800 LT.

#### **6.8.4 Narssarssuaq, Greenland**

At the close of the previous reporting period, the process of troubleshooting the transmitter had begun. In order to perform the necessary tests on the transmitter, a resistor board was shipped to the station that enabled the technician to perform tests with the Final Power Amplifier disconnected from the system. Due to the language barrier between the contractors' engineering staff and the on-site technician, Mr. Soren Larsen, the diagnostic telephone calls were channeled through the Qaanaaq technician who would then communicate with Mr. Larsen. This proved successful, however, it was determined that an on-site visit was required by the contractor. In March, Mr. Robert Gowell traveled to the Narssarssuaq station and continued troubleshooting of the system. It was found that the capacitors on the receiver tap in the Final Power Amplifier had failed and were replaced. The system was returned to an operational status. Prior to Mr. Gowell's departure the tape drive malfunctioned as well as the modem. At the close of the reporting period a replacement tape drive was sent via commercial air freight to the station.

### **6.9 May - July 1992**

#### **6.9.1 Bermuda NAS**

During the month of May, on polling the station remotely it was noticed that errors were occurring. On inspection of the system by the on-site representative it was found that the symptoms were identical to the Processor problems reported in January. A replacement card was shipped to the station. On installation of the replacement cards the defective card was found. At the close of the reporting period the station was fully operational.

#### **6.9.2 Argentina NAS**

At the start of the reporting period, the replacement chassis for the Final Power Amplifier chassis and Delay Line chassis were received. Both replacement chassis were installed into the system. Once the replacement chassis were installed, the system was restored to an operational condition.

During the second month of the reporting period the on-site representative was contacted to check out the system after we detected poor quality of the ionograms using the remote modem link-up. The on-site representative performed an internal Processor calibration with all results normal. It

was then observed that the 8A circuit breaker on the Pulse Power Supply would trip whenever the system attempted to transmit. It was noticed that the air conditioner unit in the trailer had failed creating a high temperature environment. Once the air conditioner was repaired the system was again operational.

The following week the transmitter again appeared to drop-out during the ionogram. The on-site representative observed that the Ready light on the Pulse Power Supply would begin blinking at the start of the ionogram. When the Ready set button was depressed during the running of an ionogram, the 8A breaker would trip. Due to the non-availability of test equipment to the on-site representative, all testing was restricted to visual checks. It was observed that the capacitors on the Receiver Tap in the Final Power Amplifier chassis had disintegrated. Replacing these capacitors restored the system to an operational status. Due to the downsizing of the Argentia Naval facility, the previous detachment that had loaned test equipment in support of the Digisonde maintenance had been transferred off the base. This left the on-site representative with no test equipment at all for Digisonde maintenance.

### **6.9.3 Narssarssuaq, Greenland**

At the close of the previous reporting period UMLCAR shipped a replacement tape drive to the station. At the start of this reporting period the on-site representative received and installed the tape drive. After a modification to the connectors the tape drive was placed on-line. The system remained operational for one month until the replacement tape drive malfunctioned. The failure mode was that the drive would not rewind the tape. Again, due to the language barrier, troubleshooting was conducted using the assistance of the Qaanaaq on-site engineer, Mr. Sven Erik. After approximately one month of troubleshooting it was determined that another replacement tape drive was required.

### **6.9.4 Sondre Stromfjord, Greenland**

During the reporting period an on-site visit was made to the status for the purpose of evaluating the operational status of the system and to upgrade and implement the ARTIST3 configuration.

## **6.10 August - October 1992**

### **6.10.1 Bermuda NAS**

During the reporting period the system was fully operational. The contractor did receive one call from Air Force Space Forecast Center in August stating that they were not receiving data over the

AWN. Polling the station via dial-up modem showed the system to be operating normally. The on-site representative was contacted to check the status of the AWN line. We were notified that this line was being replaced over the next two days and that is why data were not being transmitted over the AWN from the Bermuda Digisonde system.

#### **6.10.2 Argentia NAS**

During the reporting period an on-site visit was made by contractor personnel. At the close of the reporting period the system was fully operational.

### **6.11 November - January 1993**

#### **6.11.1 Bermuda NAS**

During the reporting period the system was fully operational until mid-January. At this time, one of the two transmit antenna towers of the TCI Model 613 broadband antenna collapsed as a result of one of the guy wires being caught on a Public Works truck working in the area. When the guy wire was released from the truck, the spring action caused one of the towers to fold making the antenna unusable. As a result the transmitter was shut down. At the close of the reporting period the on-site technician was attempting to temporarily suspend the radiating elements and balun in a manner that they were off the ground so that the transmitter could be turned on again to assess the feasibility of operation until a replacement tower is installed.

#### **6.11.2 Argentia NAS**

During the reporting period the system was fully operational until the last week. At that time the on-site technician informed UMLCAR that there were problems in the transmitter and tape drive. The 8A breaker on the Pulse Power Supply chassis would trip immediately on depressing the Ready button during an ionogram. On visual inspection of the transmitter the 100W amplifier was found to be covered with soot. The apparent severity of the failure required a replacement Pulse Power Supply chassis and Delay Line chassis were shipped to the station.

The tape drive required frequent resetting to remain on-line and it failed to rewind tapes properly. After several attempts the tape drive was fixed and the unit remained on-line satisfactorily at the close of the reporting period.

## **6.12 February - April 1993**

### **6.12.1 Bermuda NAS**

At the start of this reporting period, the on-site representative was able to restore some transmission by suspending the balun and a good portion of the radiating elements off the ground. The perimeter of the transmit antenna was cordoned-off with rope and hazard signs were posted warning of a radiation hazard. The low transmitter power of the system and the severe degradation of the transmit antenna caused the quality of the ionograms to be very poor. However, at times the ionograms were adequate to allow ARTIST to output scaling data on the AWN network. For this reason the system was set to continue running on a one-half hour schedule. Personnel at Falcon AFB were advised that the Bermuda data were suspect in quality. A new antenna was ordered.

### **6.12.2 Argentia NAS**

At the start of the reporting period a replacement 100W amplifier was shipped to the station. The new chassis did not rectify the fault. The original chassis were then placed back into the system. On our direction the on-site rep replaced the bridge rectifiers in the Pulse Power Supply chassis. This cleared the problem and the system was again operational with the exception that the tape drive was not fully functional. It was determined that a replacement tape drive from Phillips Laboratory was to be shipped to the station via Government channels.

Approximately two weeks after the transmitter was repaired, it was noticed on polling the station that no echoes were displayed on the ionogram.

Weather and test equipment difficulties made it impossible to find the faults. It was determined that UMLCAR personnel should travel to the station to conduct system maintenance. In the interim, a set of suspect replacement cards were sent to the station. On arrival, Mr. Gowell discovered the defective cards. In addition, both the 10 watt and 100 watt amplifiers on the back of the transmitter were defective. Replacement amplifiers were shipped to the station. Replacement of the two amplifiers restored the system to a fully operational system.

### **6.12.3 Qaanaaq, Greenland**

At the close of the reporting period, an updated diskette (dated 20 March 1993) containing the latest ARTIST3/ODDA software was sent to the station via Phillips Laboratory.

#### **6.12.4 Sondre Stromfjord, Greenland**

At the close of the reporting period, an updated diskette (dated 20 March 1993) containing the latest ARTIST3/ODDA software was sent to the station via Phillips Laboratory.

#### **6.12.5 Wallops Island, VA**

During the reporting period UMLCAR was contacted by the users of the Wallops Island DISS requesting information in solving a problem in the system. After discussions with Mr. Riley Bull the problem appeared to possibly be the result of a defective card which is not spared for the DISS systems. A loaner card was shipped down to Wallops Island to assist the on-site Air Force maintenance personnel in troubleshooting the system. On insertion of the replacement card the problem was still present in the system and the loaner card was returned to the contractor. Mr. Bull was then advised to contact Phillips Laboratory for further assistance as it appeared that possibly a card in the PC may be defective and we did not have spares. Two weeks later, we received a call from Sacramento ALC requesting information on the Rubidium frequency standard in the DISS system that was part of the authorized modifications conducted on the system in support of DORIS. After a brief discussion it was noted that the system was still operating off the Rubidium in lieu of the quartz oscillator and that the Rubidium had failed. On returning the system to the quartz oscillator the system was again fully operational.

### **6.13 May - July 1993**

#### **6.13.1 Bermuda NAS**

Data were not being received from the Bermuda station via the AWN. The station was polled via the dial-up modem and found to be working properly. The on-site technician was contacted to request the NAS Bermuda Tech Control group to verify proper operation of the AWN line on the island. The problem was identified to be on Bermuda and was corrected.

During the first week of July, UMLCAR was again contacted by Space Forecast Center that data were again not being received from the station via the AWN. On polling the station via the dial-up modem, the modem would not respond. The on-site technician was contacted and informed us that the power lines to the station were being replaced and that the power would be off for an undetermined period. The on-site technician also informed us that work had begun on replacing the 40' section of antenna tower. The following day, 9 July 1993, the on-site technician informed the contractor that the power was restored to the station and that the replacement tower section had been installed and the system was fully operational.

### **6.13.2    Argentina NAS**

A replacement tape drive arrived and was installed. This tape drive functioned properly for about one month before it began malfunctioning.

At the start of July, the system performance began to degrade with very weak echoes. After several checks, it was determined that the fault was either in the Antenna Switch chassis or the Polarization Switch boxes on the receive antennas. Initial troubleshooting of the Antenna Switch chassis showed that the 24V power supply had failed. It was determined that a replacement 24V Lambda power supply needed to be shipped to the station. These items were packaged and shipped to Argentina via Air Canada Air Cargo. On installing the new power supply the symptom did not clear. Further troubleshooting revealed that removing one of the plug-in amplifier cards in the Antenna Switch chassis for visual inspection caused the 24V power supply to work. On visual inspection of the card socket a large amount of dirt was seen. Cleaning of all card sockets returned the system to an operational status. As a preventive maintenance measure, all the "N" type connectors on the receive antenna cables were replaced. Replacement of these items returned the system to an operational status (with the exception of the intermittent tape drive) and remained operational to the close of the reporting period.

## **6.14    August - October 1993**

### **6.14.1    Bermuda NAS**

During October, UMLCAR was informed from Space Forecast Center that data were not being received from the Bermuda station via the AWN. The station was polled via the dial-up modem and found to be working properly. The on-site technician was contacted to request the NAS Bermuda Tech Control group to verify proper operation of the AWN line on the island. The problem was identified to be on Bermuda and was corrected.

### **6.14.2    Qaanaaq, Greenland**

During the reporting period one on-site visit was made by David Kitrosser (UMLCAR) and accompanied by Phillips Laboratory MSgt. Joe Whitfield and SSgt. Scott Twing. The purpose of the visit was to install an ARTIST3 computer system and to inspect the overall operational status of the Digisonde system. The new ARTIST3 computer with new firmware was installed and tested. The new fast drift cards were then installed. After correcting several small problems the system was left fully operational.

### **6.14.3 Narssarssuaq, Greenland**

During the reporting period one on-site visit was made by David Kitrosser (UMLCAR) and accompanied by Phillips Laboratory MSgt. Joe Whitfield and SSgt Scott Twing. The purpose of the visit was to inspect the overall operational status of the DISS system. Several actions were taken in various chassis to improve system performance.

On leaving Narssarssuaq the DISS was fully operational with the exception of antenna #5. Shortly after leaving the station a failure was reported in the Processor chassis with maintenance action deferred to the next reporting period.

### **6.14.4 Sondre Stromfjord, Greenland**

During the reporting period an on-site visit was made by David Kitrosser (UMLCAR) and accompanied by Phillips Laboratory MSgt. Joe Whitfield and SSgt Scott Twing. The purpose of the visit was to inspect the overall operational status of the DISS system.

An overall check of the system was performed with the 14 tubes in the Final Power Amplifier chassis replaced. A standard drift calibration was performed.

According to the flight service station at the local airport, the critical aviation HF frequencies are 2.950, 5.526, 8.945, and 10.02 MHz. The restricted frequency list in the input computer now has 2.95, 5.00, 5.50, 5.55, 8.95, 10.00, 10.05 and 15.00 marked. Bear in mind that the restricted frequency algorithm has been modified as of August 1993 and now entering a frequency into the table will protect that frequency +/- 25 kHz. The algorithm takes into account the frequency search offset and transmitter bandwidth.

At the close of the reporting period the system was fully operational.

## **6.15 November - January 1994**

### **6.15.1 Bermuda NAS**

In January, UMLCAR was contacted by Space Forecast Center (SFC) and informed that they had not been receiving data from the Bermuda Digisonde since mid-December. The station was polled via the dial-up modem and found to be working. The contractor then faxed a copy of an ionogram and the AWN message to SFC. After review of the fax by SFC it was determined that Tinker AFB had deleted the MANOP header for Bermuda preventing the communications system from



recognizing the Bermuda messages. After entering the Bermuda MANOP header into the communications system, data were again received at SFC.

## **6.16 February - May 1994**

### **6.16.1 Bermuda NAS**

On routine polling of the station in March, it was found that the ionograms were weak below 4MHz. The on-site technician was contacted and requested to perform a calibration ionogram. Results of the calibration appeared normal. Further investigation revealed that the capacitors on the Receiver Tap in the Final Power Amplifier chassis had blown. The capacitors were replaced as well as a new set of fourteen tubes were installed. The system was returned to an operational status.

### **6.16.2 Argentia NAS**

At the close of the previous reporting period, the on-site technician, Mr. Dan Enright, had contacted us that the Final Power Amplifier had failed. A replacement chassis was installed bringing the system back to an operational status.

During March/April an ARTIST3 system was shipped to the station. The ARTIST3 system is a 486 based PC with cartridge drive and color monitor that is designed to replace the older 286 ARTIST computer and Pertec tape drive. On arrival at the station there was visible damage, as a result of shipping, to the computer case and cartridge drive. On power-up the PC worked, but the tape drive did not as the damage prevented insertion of a tape cartridge.

In May, it was determined that UMLCAR personnel were required to travel to Argentia to perform an overall system check and to repair the ARTIST3 system. At the close of the reporting period the station was returned to an operational status.

## **6.17 June - August 1994**

No maintenance was performed during this period.

## **6.18 September - November 1994**

### **6.18.1 Argentina, NAS**

During the reporting period an on-site visit was made by David Kitrosser (UMLCAR) and accompanied by Phillips Laboratory MSgt. Joe Whitfield and Capt. Hughes. The purpose of the visit was to remove the Digisonde 256 and replace it with a Sacramento baselined DISS and perform system check-out.

Several days prior to arrival on-site by David Kitrosser, an unusual thunderstorm passed through the area. Lightning struck the ground approximately 200 feet from the receive antenna array. Several of the Antenna Switch front end cards had defective 3 ohm current monitoring/protection resistors. One card had evaporated. Only one of the seven antenna polarization switch boxes survived. The boxes from the old Digisonde 256 were used and the defective antenna boxes were returned to Phillips Laboratory for bench repair. At the close of the reporting period, the system was fully operational.

### **6.18.2 Goose Bay, Labrador**

During the reporting period one on-site visit was made by David Kitrosser (UMLCAR). The purpose of the visit was to inspect the overall operational status of the DISS system. Several actions were taken in various chassis to improve performance. We replaced ARTIST3 software with the official AWS ARTIST3 software. At close of the reporting period, the system was fully operational.

## **6.19 December - February 1995**

No maintenance actions were performed during the reporting period.

## **6.20 March - May 1995**

No maintenance actions were performed during the reporting period.

## **6.21 June - August 1995**

### **6.21.1 Goose Bay, Labrador**

In July 1995 Mr. Balgit Gill, Goose Bay station manager, attended the Digisonde Training Seminar conducted at the UMLCAR facility in Lowell and brought with him cards which showed

damage from acid dripping for a defective power supply capacitor. The station was not operating at that time and required a visit by UMLCAR personnel. In August, Mr. David Kitrosser traveled to the station and repaired the system.

#### **6.21.2    Argentina NAS**

In August, Mr. David Kitrosser traveled to the station to make necessary repairs. On arrival it was noted that the station shelter leaked very badly. The shelter was dried as good as possible. Continued maintenance actions revealed that the ARTIST computer had failed. No replacement was available during the visit.

### **6.22    September - November 1995**

#### **6.22.1    Korea, Osan Air Base**

A visit to the DISS site was carried out by D. Kitrosser. Two of the receive antennas are installed on 15 foot concrete pillars with an "X" cross section so that it is possible to walk out to the corners of the antennas. Using drift, it did seem that the signals from these antennas were a little weaker. The phase appeared to be within 22.5 degrees of the other antennas. Terence Bullett had noticed the same effects for elevated antennas at other sounder installations.

The TCI transmit antenna was installed on a slope, approximately 12 to 15 degrees. While UMLCAR was there, the base civil engineers came to the site with earth moving equipment and made the slope 8 degrees. The slope, although it should have been avoided, does not appear to seriously interfere with the antenna performance.

The 12-volt power supply in the antenna switch appeared to shut down, at first every few hours, then approximately every 10 minutes. The radio shop on base provided a variable voltage, 0.9 ampere power supply which, although would not supply enough current by itself, when hooked in parallel with the defective supply, prevented the defective power supply from shutting down. It appears that the power supply is overloaded or defective.

It was necessary to install a low-pass filter between the antenna switch and the processor chassis. There were multiple interferors at 980 kHz, 1.12 MHz, 1.32 MHz. The design has been used several times previously. In addition, at night there were strong interferors at 3.92 and 4.02 MHz which could be prevented from saturating the input stages only by reducing the gain of the antenna pre-amps as low as possible by removing the gain resistors entirely.

The telephone lines to the sounder (one dial-up line plus the AWN connection) were connected. The dial-up line appeared to be a solid connection based on the voice quality. The AWN modem was receiving other polls and responses on the multi-drop circuit and would probably work as soon as Sacramento could convince Tinker AFB to start polling Osan. Coordinates of the sounder are 37.05N, 127.03E.

## **6.23 December - February 1996**

### **6.23.1 Bermuda NAS**

The purpose of this visit to the Bermuda NASA Tracking Station was to solve the interference problem. Harbour Radio has been complaining about interference on the International Marine Distress Frequency, 2.182 MHz ever since the new DISS was installed approximately six months ago. The interference lasted for the entire sweep, not just near the 2.182 MHz. Study of the radiation from the sounder, using both digital and analog spectrum analyzers connected to antennas at the NASA site and also connected to the 150 watt exciter output through a probe, did not show energy at 2.182 MHz much above the floor of the spectrum analyzers, but these spectrum analyzers do not work well with our pulsed signal. A 10 MHz WWV receiver at the NASA site always showed strong interference from the sounder, even after repairing the sounder. It was concluded that the WWV receiver simply had a very poor front end. The 2.182 MHz notch filter design by Dr. Bibl was installed in the output of the final amplifier of the transmitter.

The primary cause of the interference to Harbour Radio on the Marine Distress frequency of 2.182 MHz was determined to be a defective 10 watt amplifier in the exciter chassis. This was determined by having Harbour Radio listen during several tests. When we disconnected the output of the 10 watt amplifier from the 150 watt amplifier, the interference went away. When we disconnected the input of the 10 watt amplifier from the processor chassis, the interference persisted. We swapped the amplifier with a spare and the interference occurred only at some frequencies, not over the whole ionogram sweep. Incidentally, we tried running the defective amplifier from 24 volts DC rather than from the normal pulsed power. That did reduce the interference somewhat, but not as much as swapping the defective amplifier for a good one running on pulsed power.

UMLCAR put back the attenuators which were originally installed with the DGS256 in the late 1980s. One was a fixed 12 dB attenuator and the other a 10 dB attenuator at lower frequencies decreasing to about 5 dB at frequencies above 10 MHz. The Bird Power meter indicated around 2.5 kW. The quality of the ionograms was quite good even with low power, probably due to little local interference. After many telephone calls to Harbour Radio with the generous assistance of

various Harbour Radio operators, we determined that each of these steps reduced the perceived interference.

There were a couple of ionograms with multiple E-layers up to 6<sup>th</sup> hop. Based on study of these multiple layers on the printer output it was decided to lower the height of the echo traces by 5 km. The "lateness" of the transmitter is contributed to the long cable to the transmitter antenna.

#### **6.24 March - May 1996**

There were no maintenance actions this reporting period.

#### **6.25 June - August 1996**

There were no maintenance actions during this period.

### **7. Publications and Reports from this Contract**

- Anderson, D.N., M.J. Buonsanto, M. Codrescu, D. Decker, C.G. Fesen, T.J. Fuller-Rowell, B.W. Reinisch, P.G. Richards, R.G. Roble, R.W. Schunk, and J.J. Sojka, Intercomparison of physical models and observations of the ionosphere, *J. Geophys. Res.*, in print, 1997.
- Buchau, J., G.S. Sales, S. Dandekar, B. Weijers, and D. Reynolds, The effects of multihop HF propagation on the performance of TH backscatter radars, AGARD Conference Proceedings, 543, July 1994.
- Cannon, P.S., B.W. Reinisch, J. Buchau and T.W. Bullett, Response of the Polar Cap F Region Convection Direction to changes in the Interplanetary Magnetic Field: Digisonde Measurements in Northern Greenland, *J. Geophys. Res.*, 96(A2), 1239-125, 1991.
- Cannon, P.S., Crowley, G., Reinisch, B.W. and Buchau, J., "Digisonde Measurements of Polar Cap Convection for Northward Interplanetary Magnetic Field," *J. Geophys. Res.*, 97, 16,877, 1992.
- Chen, C.F., B.W. Reinisch, J.L. Scali, X. Huang, R.R. Gamache, M.J. Buonsanto, and B.D. Ward, The accuracy of ionogram-derived N(h) profiles, *Adv. Space Res.*, 14(12), 43-46, 1994.
- Colerico, M., M. Mendillo, D. Nottingham, J. Baumgardner, J. Meriwether, J. Mirick, B.W. Reinisch, J.L. Scali, C.G. Fesen, and M.A. Biondi, Coordinated measurements of F region dynamics related to the thermospheric midnight temperature maximum, *J. Geophys. Res.*, 101(A12), 26,783-26,793, 1996.
- Crowley, G., P.S. Cannon, C.G. Dozois, B.W. Reinisch and J. Buchau, Polar cap convection for Bz northward, *Geophys. Res. Lett.*, 19(7), 657-660, 1992.
- Galkin, I.A., B.W. Reinisch, G.A. Osokov, E.G. Zaznobina, and S.P. Neshyba, Feedback neural networks for ARTIST ionogram processing, *Radio Sci.*, 31(5), 1119-1128, 1996.

- Huang, X., B.W. Reinisch, and W.S. Kuklinski, Mid-point electron density profiles from oblique ionograms, *Annali di Geofisica*, Vol. XXXIX, No. 4, 1996.
- Huang, X., and B.W. Reinisch, Vertical electron density profiles from Digisonde ionograms. The average representative profile, *Annali di Geofisica*, Vol. XXXIX, No. 4, 1996.
- Mendillo, M., J. Baumgardner, D. Nottingham, J. Aarons, B.W. Reinisch, J.L. Scali, and M. Kelley, Imaging science investigations of thermospheric-ionospheric dynamics at the Arecibo Observatory, *J. Geophys. Res.*, in print, 1997.
- Reinisch, B.W., D.M. Haines, and W.S. Kuklinski, The new portable Digisonde for vertical and oblique sounding, AGARD Conf. Proc., No. 502, 11-1 to 11-11, 1992.
- Reinisch, B.W., X. Huang, and G.S. Sales, Regional ionospheric nowcasting, Solar-Terrestrial Predictions IV, Proc. of Workshop, Ottawa, Canada, 1992.
- Reinisch, B.W., X. Huang, and G.S. Sales, Regional ionospheric mapping, *Adv. Space Res.*, 13(3), 45-48, 1993.
- Reinisch, B.W., D.N. Anderson, R.R. Gamache, X. Huang, C.F. Chen, and D.T. Decker, Validating ionospheric models with measured electron density profiles, *Adv. Space Res.*, 14(12), 67-70, 1994.
- Reinisch, B.W., and C.F. Chen, New input to IRI from the worldwide Digisonde network, *Adv. Space Res.*, 14(12), 27-36, 1994.
- Reinisch, B.W., T.W. Bullett, and J.L. Scali, High latitude Digisonde measurements and their relevance to IRI, *Adv. Space Res.*, 16(1), 17-26, 1995.
- Reinisch, B.W. and X. Huang, The F1 ledge: density, height and slope, *Annali di Geofisica*, Vol. XXXIX, No. 4, 1996.
- Reinisch, B.W., and X. Huang, Low latitude Digisonde measurements and comparison with IRI, *Adv. Space Res.*, 18(6), 5-12, 1996,
- Reinisch, B.W., and X. Huang, The F1 region at 170 km, *Adv. Space Res.*, 18(6), 153-156, 1996.
- Reinisch, B.W., D.M. Haines, K. Bibl, I. Galkin, X. Huang, D.F. Kitrosser, G.S. Sales, and J.L. Scali, Ionospheric sounding in support of OTH radar, *Radio Sci.*, in print, 1997.
- Sales, .S., I.G. Platt, D.M. Haines, U. Huang, and J.L. Heckscher, Modeling and design for a new ionospheric modification experiment, AGARD Conference Proceedings, 485, May 1990.
- Sales, G.S., B.W. Reinisch, J.L. Scali, C. Dozois, T.W. Bullett, E.J. Weber, and P. Ning, Spread F and the structure of equatorial ionization depletions in the southern anomaly region, *J. Geophys. Res.*, 101(A12), 26819-26827, 1996.
- Scali J.L., Reinisch, B.W., C.J. Heinselmann and T.W. Bullett, Coordinated Digisonde and incoherent scatter radar F region drift measurements at Sondre Stromfjord, *Radio Sci.*, 30(5), 1481-1498, 1995.
- Scali, J.L., and B.W. Reinisch, F-region drift velocities in the dusk sector mid-latitude trough, *J. Atmos. & Terres. Phys.*, 57(9), 1045-1056, 1995.

Scali, J.L., and B.W. Reinisch, Geomagnetic storm time studies using Digisonde data, *Adv. Space Res.*, in print, 1997.

Wang, Chunnian, X. Huang, B.W. Reinisch, and J.A. Klobuchar, Deriving the total electron content from ionograms, Proceedings of the International Beacon Satellite Symposium, Aberystwyth, UK, July 1994.

Wojtal, J.P., Correlation Analysis of FoF2 data and its application to ionospheric mapping, M.S. thesis, University of Massachusetts Lowell, Dept. of Electrical Engineering, 1991.

## **Reports**

ADEP (ARTIST Data Editing and Printing) Manual, Version 2.12, University of Massachusetts Lowell, Center for Atmospheric Research, July 1994.

Gamache, R.R., and B.W. Reinisch, Ionospheric characteristics for archiving at the World Data Centers, GL-TR-90-0215, December 1990, ADA236645.

Gamache, R.R., and W.T. Kersey, A comparison of manual scaled and predicted foE and foF1 critical frequencies, GL-TR-90-0214, July 1990, ADA235551.

Kuklinski, W., J. Hazelwood, and B.W. Reinisch, Digital oblique remote ionospheric sensing (DORIS) program development, PL-TR-92-2113, April 1992, ADA261750.

Reinisch, B.W., X. Huang, and G.S. Sales, Data driven ionospheric mapping technique for wide area nowcasting, PL-TR-91-2258, September 1991, ADA258601.

Sales, G.S., High frequency (HF) radiowave propagation, PL-TR-92-2123, April 1992, ADA261726.

Sales, G.S., OTH-B radar system: system summary, PL-TR-92-2134, May 1992, ADA261727.

Scali, J.L., and B.W. Reinisch, Measurements of F-region drift velocities at the dusk sector mid-latitude trough, PL-TR-92-2094, 1992, ADA257766.

Scali, J.L., The mid-latitude trough. A review, PL-TR-92-2100, 1992, ADA258606.

Scali, J.L., A quality control package for the Digisonde drift analysis (DDA), PL-TR-93-2220, 1993, ADA278663.

Scali, J.L., B.W. Reinisch, and C.G. Dozois, Polar convection monitoring determination of the IMF BZ and BY orientations from Digisonde drift velocities, PL-TR-95-2138, August 1995, ADA305419.

Tang, Jane, C.G. Dozois, and R.R. Gamache, ARTIST tape output formats, GL-TR-90-0190, July 1990, ADA235173.

## 8. References

- Akram, A., High latitude ionospheric flow studies, PhD. thesis, Imperial College, London, UK, 1992.
- Buchau, J., B.W. Reinisch, D.N. Anderson, E.J. Weber, and C. Dozois, Polar cap plasma convection measurements and their relevance to the modeling of the high-latitude ionosphere, *Radio Sci.*, 23(4), 521-536, 1988.
- Cannon, P.S., B.W. Reinisch, J. Buchau and T.W. Bullett, Response of the Polar Cap F Region Convection Direction to changes in the Interplanetary Magnetic Field: Digisonde Measurements in Northern Greenland, *J. Geophys. Res.*, 96(A2), 1239-125, 1991.
- Cerveney, V., and I. Psencik, Gaussian beams and paraxial ray approximation in three-dimensional elastic inhomogeneous media, *J. Geophys. Res.*, 53, 1-15, 1983.
- Cerveney, V., Gaussian beams synthetic seismograms, *J. Geophys. Res.*, 58, 44-72, 1985.
- Crowley, G., P.S. Cannon, C.G. Dozois, B.W. Reinisch and J. Buchau, Polar cap convection for Bz northward, *Geophys. Res. Lett.*, 19(7), 657-660, 1992.
- Gamache, R.R., and B.W. Reinisch, Proceedings for the international workshop on Digital Ionogram Data Formats for World Data Center Archiving, University of Massachusetts Lowell, Center for Atmospheric Research, November 1989.
- Gamache, R.R. and Reinisch, B.W., Databasing of Scientific Data, Proceedings of the Workshop on Geophysical Informatics, Moscow, Russia, WDC-A Report UAG-99, 102-108, 1991.
- Hairston, M.R. and R.A. Heelis, Model of the High-latitude Ionospheric Convection Pattern During Southward Interplanetary Magnetic Field Using DE-2 Data, *J. Geophys. Res.*, 95, 2-2343, 1990.
- Heelis, R.A., J.K. Lowell, and R.W. Spiro, A model of the high-latitude ionospheric convection pattern, *J. Geophys. Res.*, 87(A8), 6339-6365, 1982.
- Heppner, J.P. and N.C. Maynard, Empirical models of high latitude electric field models, *J. Geophys. Res.*, 92, 4467-4489, 1987.
- Huang, X., and B.W. Reinisch, Vertical electron density profiles from the Digisonde network, *Adv. Space Res.*, 18(6), 121-129, 1996.
- Huang, X., B.W. Reinisch, and W.S. Kuklinski, Mid-point electron density profiles from oblique ionograms, *Annali di Geofisica*, Vol. XXXIX, No. 4, 1996.
- Kuklinski, W., J. Hazelwood, and B.W. Reinisch, Digital oblique remote ionospheric sensing (DORIS) program development, PL-TR-92-2113, April 1992, ADA261750.
- Piggott, W.R., and K. Rawer, Editors, URSI Handbook of Ionogram Interpretation and Reduction, World Data Center A for Solar-Terrestrial Physics Report UAG-23 and 23A, Boulder, CO, 1978.



- Porter, M.B., and H.P. Bucker, Gaussian beam tracing for computing ocean acoustic fields, *J. Acous. Soc. Am.*, 82(4), 1349-1359, 1987.
- Reinisch B.W., J Buchau and E.J. Weber, Digital ionosonde observations of the polar cap F region convection, *Phys. Scri.*, 36, 372-377, 1987.
- Reinisch, B.W., D.M. Haines, and W.S. Kuklinski, The new portable Digisonde for vertical and oblique sounding, AGARD Conf. Proc., No. 502, 11-1 to 11-11, 1992.
- Reinisch, B.W., X. Huang, and G.S. Sales, Regional ionospheric mapping, *Adv. Space Res.*, 13(3), 45-48, 1993.
- Reinisch, B.W., and C.F. Chen, New input to IRI from the worldwide Digisonde network, *Adv. Space Res.*, 14(12), 27-36, 1994.
- Reinisch, B.W., T.W. Bullett, and J.L. Scali, High latitude Digisonde measurements and their relevance to IRI, *Adv. Space Res.*, 16(1), 17-26, 1995.
- Rush, C.M., Improvement in ionospheric forecasting capability, AFCRL-72-0138, Feb.1972, AD742258.
- Sales, G.S., Specular Scatter: A New Mechanism for Ionospheric Backscatter, AGARD Conference Proceedings, No. 419, May, 1987.
- Sales, G.S., High frequency (HF) radiowave propagation, PL-TR-92-2123, April 1992, ADA261726.
- Sales, G.S., OTH-B radar system: system summary, PL-TR-92-2134, May 1992, ADA261727.
- Scali, J.L., The mid-latitude trough. A review, PL-TR-92-2100, 1992, ADA258606.
- Scali J.L., Reinisch, B.W., C.J. Heinselmann and T.W. Bullett, Coordinated Digisonde and incoherent scatter radar F region drift measurements at Sondre Stromfjord, *Radio Sci.*, 30(5), 1481-1498, 1995.
- Scali, J.L., B.W. Reinisch, and C.G. Dozois, Polar convection monitoring determination of the IMF BZ and BY orientations from Digisonde drift velocities, PL-TR-95-2138, August 1995, ADA305419.
- Scali, J.L., B.W. Reinisch, and T.W. Bullett, Geomagnetic storm time studies using Digisonde data, *Adv. Space Res.*, (in print), 1997.
- Sojka, J.J., C.E. Rasmussen and R.W. Schunk, An interplanetary magnetic field dependent model of the ionospheric convection electric field, *J. Geophys. Res.* 91, 11281-1129, 1986.
- Wojtal, J.P., Correlation Analysis of FoF2 data and its application to ionospheric mapping, M.S. thesis, University of Massachusetts Lowell, Dept. of Electrical Engineering, 1991.